MIT JOINT PROGRAM
SCIENCE POLICY
GLOBAL CHANGE

Report 368
*August 2023*

# The Changing Nature of Human-Forced Hydroclimatic Risks across Africa

C. Adam Schlosser, Andrei Sokolov, Xiang Gao, Tim Thomas and Ken Strzepek

**MIT Joint Program on the Science and Policy of Global Change** combines cutting-edge scientific research with independent policy analysis to provide a solid foundation for the public and private decisions needed to mitigate and adapt to unavoidable global environmental changes. Being data-driven, the Joint Program uses extensive Earth system and economic data and models to produce quantitative analysis and predictions of the risks of climate change and the challenges of limiting human influence on the environment—essential knowledge for the international dialogue toward a global response to climate change.

To this end, the Joint Program brings together an interdisciplinary group from two established MIT research centers: the **Center for Global Change Science (CGCS)** and the **Center for Energy and Environmental Policy Research (CEEPR)**. These two centers—along with collaborators from the Marine Biology Laboratory (MBL) at Woods Hole and short- and long-term visitors—provide the united vision needed to solve global challenges.

At the heart of much of the program's work lies MIT's Integrated Global System Model. Through this integrated model, the program seeks to discover new interactions among natural and human climate system components; objectively assess uncertainty in economic and climate projections; critically and quantitatively analyze environmental management and policy proposals; understand complex connections among the many forces that will shape our future; and improve methods to model, monitor and verify greenhouse gas emissions and climatic impacts.

This report is intended to communicate research results and improve public understanding of global environment and energy challenges, thereby contributing to informed debate about climate change and the economic and social implications of policy alternatives.

***—Ronald G. Prinn,***
*Joint Program Director*

**MIT Joint Program on the Science and Policy of Global Change**

Massachusetts Institute of Technology
77 Massachusetts Ave., E19-411
Cambridge MA 02139-4307 (USA)

**T** (617) 253-7492 **F** (617) 253-9845
globalchange@mit.edu
http://globalchange.mit.edu/

GLOBAL CHANGE

AUGUST 2023

# The Changing Nature of Human-Forced Hydroclimatic Risks across Africa

C. Adam Schlosser[1], Andrei Sokolov[1], Xiang Gao[1], Tim Thomas[2] and Ken Strzepek[1]

**Abstract:** We present results from large ensembles of projected 21st century changes in seasonal precipitation and near-surface air temperature over Africa and selected sub-continental regions. These ensembles are a result of combining Monte Carlo projections from a human-Earth system model of intermediate complexity with pattern-scaled responses from climate models of the Coupled Model Intercomparison Project Phase 6. These future ensemble scenarios consider a range of global actions to abate emissions through the 21st century. We evaluate distributions of surface-air temperature and precipitation change. In all regions, we find that without any emissions or climate targets in place, there is a greater than 50% likelihood that mid-century temperatures will increase threefold over the current climate's two-standard deviation range of variability. However, scenarios that consider more aggressive climate targets all but eliminate the risk of these salient temperature increases. A preponderance of risk toward decreased precipitation exists for much of the southern Africa region considered, and this is also compounded by enhanced warming (relative to the global trajectory). Over eastern and western Africa, the preponderance of risk in increased precipitation change is seen. Strong climate targets abate evolving regional hydroclimatic risks. Under a target to limit global climate warming to 1.5˚C by 2100, the risk of precipitation changes within Africa toward the end of this century (2065-2074) is commensurate to the risk during the 2030s without any global climate target. Thus, these regional hydroclimate risks over much Africa could be delayed by 30 years, and in doing so, provide invaluable lead-time for national efforts to prepare, fortify, and/or adapt.



1 Joint Program on the Science and Policy of Global Change, MIT, Cambridge, MA
2 International Food Policy Research Institute (IFPRI), Washington, DC

## 1. Introduction

Africa is faced with the very real threat of substantial human-forced climate changes in the coming decades. Geographically, Africa is a remarkable continent and presents some of the most challenging features with a total landscape that spans across the Northern and Southern Hemispheres and covers climate and weather regimes characterized by the tropics, sub-tropics, and extra-tropics. Africa's climate and weather systems are interconnected across these regimes and therefore challenge the use of climate models to identify and predict specific emerging patterns that will result from human-forced global changes. These uncertainties necessitate a comprehensive sampling of the many plausible outcomes that may occur in the future, and the use of global climate models such that the important teleconnections across the tropics, sub-tropics, and extra-tropics can be explicitly represented. While efforts to provide the most spatially refined information will ultimately be crucial to providing local/location-based guidance for stakeholders, the modeling tools by which this information can be delivered (i.e. regional climate models) continue to suffer from the inability to comprehensively sample across structural uncertainties in prediction. As such, our ability to rigorously qualify and quantify the distributions and likelihood of regional climate outcomes presently rely upon methods that incorporate rigorous sampling of global-scale uncertainties in the human-forced climate response and translating how these manifests into regional outcomes. Comprehensive assessments of the global climate sensitivity using traditional climate models are untenable, and therefore we must rely on reduced form models to assign boundaries and sampling distributions (e.g., Sokolov *et al.*, 2018 and Libardoni *et al.*, 2018). Further, these large-ensemble simulations should also consider several different scenarios that consider a range of global emissions pathways and/or climate targets (e.g., Morris *et al.*, 2021), and provide spatial details that are commensurate to the requirements for regional impact studies (e.g., Pierce *et al.*, 2009).

In view of these considerations, we employ a hybridization of Earth-system models to analyze the likelihood of changes in precipitation and surface-air temperature in the coming decades and into the latter half of this century for the greater southern Africa region with a regional emphasis over Africa. We employ a technique (Schlosser *et al.*, 2012) that constructs large ensembles of plausible climate change. This method combines plausible patterns of human-forced regional climate change with a comprehensive assessment of the global climate change response as determined by the MIT Integrated Global System Model (Paltsev and Schlosser, 2021). We evaluate the resultant distributions over three selected regions over Africa that correspond with notable climatic features. We identify the salient shifts in these derived distributions from a reference emission scenario to moderate to aggressive climate-stabilization policies. We close with summary remarks and discussion of ongoing work and applications.

## 2. Assessment of regional Climate shifts

### 2.1 Region of Study and Variables of Interest

The overall area of study (**Fig. 1**) is an extension and compliment to prior work (Schlosser *et al.*, 2021; Arndt *et al.*, 2019; Schlosser and Strzepek, 2015; and Fant *et al.*, 2015) that provide multi-sector socio-economic-environmental assessments of climate risks for developing nations across Africa, and the effectiveness of low-carbon pathways to reduce risks. This study will present a screening-level assessment of potential climate shifts over Africa and focus on two key hydro-climatic variables: precipitation and near-surface air temperature ($T_a$). At a screening level assessment, we will focus our analyses on area-averaged, distributional changes over three large sub-regions of Africa (denoted in Fig. 1): Eastern Africa (EAfr), West Central Africa (WCA), and Southern Africa (SAfr). A description of the model experimentation and methodology is provided in the next section. Below we describe some of the seasonal features of $T_a$ and precipitation of the current climate that are aligned and distinguish our three regional areas of focus. Our historical assessment is based on the observations taken from the Global Precipitation Climatology Project (GPCP, Huffman *et al,* 2009, and updates by Adler *et al.*, 2018) as well as $T_a$ from the Climate Research Unit (CRU, e.g., Osborn *et al.*, 2014).

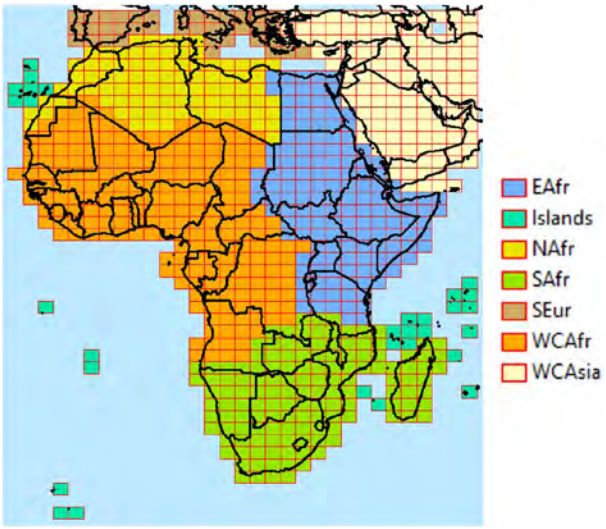


**Figure 1.** Map of the study region considered in this study. The major sub-regions of Africa are also indicated by the color shaded grids. These sub-regions are also used as the basis for the area-averaged results presented in the analyses.

Among the three regions considered, the SAfr region is distinguished by the strongest amplitude in the annual cycle of (seasonally averaged) precipitation (**Fig. 2**), and during its colder seasonal periods experiences the lowest rates of precipitation among the three regions considered in this study. The strongest degree of interannual variability occurs during the spring season periods. In contrast, the EAfr and WCA regions experience notably smaller annual-cycle amplitudes in precipitation, but like SAfr, their highest precipitation rates occur during the summer periods, with (weaker) dry periods in their winter periods. The seasonality of $T_a$, in terms of amplitude, exhibits more consistency across the regions compared to precipitation (Fig. 2). The most notable distinction among the three regions is that SAfr experiences the coldest seasonal temperatures and is mostly likely a result of its landscape being located at the higher latitudes (than EAfr and WCA).

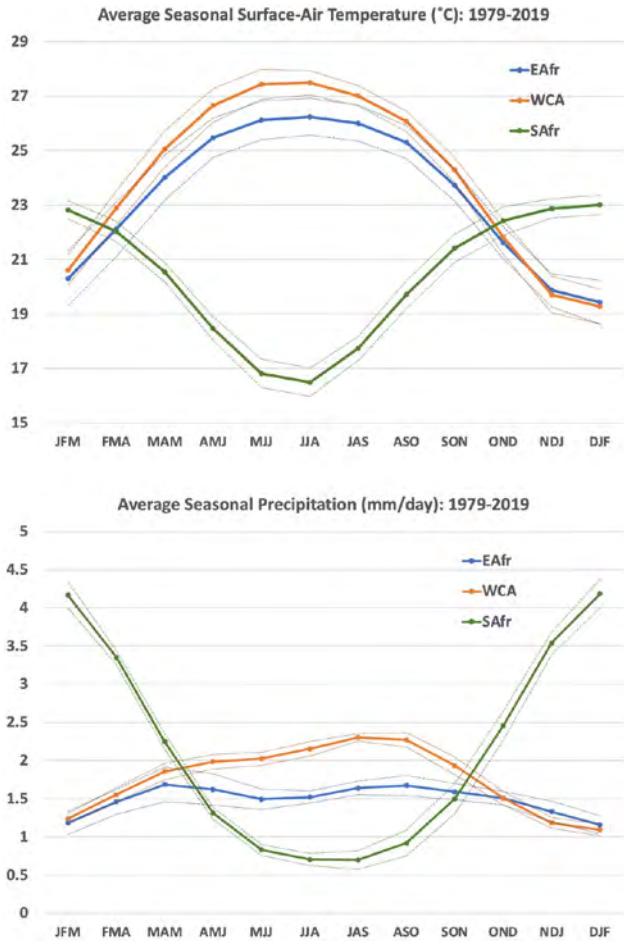


**Figure 2.** Running seasonally averaged (1979–2009) maps of surface-air temperature (top panel) and precipitation (bottom panel). Surface-air temperature is in units of ˚C and based on the Climate Research Unit (CRU, Jones *et al.*, 1999) data archive. Precipitation is in units of mm/day and based on the data from the Global Precipitation Climatology Project (GPCP, Huffman *et al.*, 2007). The results are shown as area-weighted averages for three sub-regions of focus: eastern (EAfr), western-central (WCA), and southern (SAfr) Africa (refer to Fig. 1 for the mapping of these domains). The solid lines indicate the mean values and the lighter dotted lines indicate the plus/minus one standard-deviation of their inter-decadal variability.

In order to gauge a degree of salience to the changes produced by the ensemble scenarios of change (described in the next sections), we have also assessed the *interdecadal* standard deviation of the seasonal, area-averaged quantities (**Table 1**, in italics). For surface-air temperature, the standard deviations are similar across seasons and the regions. For precipitation, overall the degree of variability is consistent across the regions and seasons, with a salient exception over SAfr during the summer periods (about twice as high). In our assessment of the distribution of changes across the 21st century (Section 2.4), we will highlight the portions of the distributions that are in exceedance to these variance statistics, and in this way, represent the risk of salient change. It should be noted that the limited temporal extent of these historical data sets may affect the robustness of our inter-decadal variance estimates.

## 2.2 Scenarios of Global Change

The set of scenarios for this study was selected from the *2021 Food, Energy, Water, and Climate Outlook* (Paltsev and Schlosser, 2021) produced by the MIT Joint Program on the Science and Policy of Global Change using the Integrated Global System Model (IGSM) framework. Each IGSM scenarios consist of a large ensemble of 400 members. The ensemble provides a multi-dimensional Latin-Hypercube sampling that spans the plausible Earth systems' response to natural and anthropogenic drivers, with the sampling boundaries determined by observations (e.g., Sokolov *et al.*, 2018 and Libardoni *et al.*, 2018). It also spans a range of global emissions policies and are based on a regionally

**Table 1.** Mean (bold) and standard deviations (italics) of area-averaged precipitation and surface-air temperature for the Eastern, West Central, and eastern South Africa regions (EAfr, WCA, and SAfr respectively) of study. Results are presented for two seasonal mean periods: December-February (DJF) and June-August (JJA). The diagnostics of precipitation (units in mm/decads, decad=10 days) are based on the Global Precipitation Climatology Project (units in ˚C), and surface-air temperature is based on observations assembled by the Climate Research Unit (CRU). See text for citations to data. Statistics span the years 1979-2019, and note that the standard deviation estimates are based across decadal means for each season so as to serve as a baseline for the decadal mean changes assessed in the 21st century scenario projections.

| | | EAfr | WCA | SAfr |
|---|---|---|---|---|
| **Precipitation** | DJF | **11.5** ± *0.5* | **10.9** ± *0.4* | **41.8** ± *0.9* |
| | JJA | **15.2** ± *0.4* | **21.5** ± *0.5* | **7.0** ± *0.4* |
| **Temperature** | DJF | **19.4** ± *0.4* | **19.3** ± *0.3* | **23.0** ± *0.2* |
| | JJA | **26.3** ± *0.3* | **27.5** ± *0.3* | **16.5** ± *0.3* |

detailed, multi-sector, economy-wide model that includes pricing of fossil fuels, fossil resources, and vintage capital in capital intensive sectors (e.g., Chen *et al.*, 2016). Under the policy scenarios that are described below, prematurely retired capital stock and the need to replace conventional energy sources with more expensive, low-carbon options draw investment resources away from other sectors of the economy and, thus, have an impact on GDP growth in mitigation scenarios. However, it is reallocated toward those energy sources that meet the emissions reduction targets at least cost. Four scenarios, developed to span a range of possible global actions to abate greenhouse gas emissions over the coming century, were used to explore climate-change risks.

**Baseline with Covid (BASECOV):** This scenario has no explicit climate mitigation policies anywhere in the world. Thus, it represents a world in which there is no Paris Agreement and no alternative action towards reducing emissions for the sake of limiting climate change. However, it includes some energy policies such as fuel economy standards, renewable electricity requirements, and the gradual phase-out of old coal power plants that are presently occurring with various motivations. These motivations include reducing imported oil dependence, using less of exhaustible resources, or to reducing conventional pollutants. In the 2021 Outlook, we include an assessment of Covid-19 impacts on economic growth, energy, and emissions. The Covid-19 pandemic is projected to have a short-term direct impact on greenhouse gas (GHG) emissions. For near-term economic growth projections (up to 2030, including impacts from Covid-19), we rely on our recent analysis (Reilly *et al.*, 2021); for medium-term projections (up to 2050), we use OECD (2020) and IEA (2020) forecasts. For GDP growth rates after 2050, we assume constant productivity growth profiles based on the corresponding region-specific rates in mid-century. The BASECOV serves as a baseline scenario because of its simplicity. Metrics from the other scenarios are often presented as the difference between another scenario and the BASECOV scenario. It provides the upper assessment of our modeled physical risks.

**Paris Forever with Covid (PFCOV):** Countries meet the mitigation targets in their Nationally Determined Contributions (NDCs) and continue to abide by them through the end of the century. The Paris Agreement includes NDCs submitted at the 2015 Paris Conference of the Parties (COP) of the Framework Convention on Climate Change (FCCC). These NDCs—aimed at the reduction of $CO_2$ and other GHG emissions—generally deepened and extended through 2030 those made at the 2009 Copenhagen COP through 2020. These reductions are typically expressed as (1) an absolute emissions target (ABS), measured as an annual level of emissions measured in Mt, (2) a percentage reduction from a pre-determined baseline, which can easily be converted into an absolute emissions target, or (3) an emissions intensity target (INT), measured as emissions in relation to GDP.

**Paris2C:** This scenario aims to limit climate warming to no higher than a 2˚C global average at 2100. This is achieved by implementing a globally coordinated, smoothly rising carbon price – such that emissions are reduced. Variations in mitigation policies result in the overall uncertainty of different patterns of resource and energy use, different choices of technology, and drag on overall economic growth. This is also combined with the uncertainty of the global climate response that is represented in the MIT Earth System Model (MESM, Sokolov *et al.*, 2019). As described in Reilly *et al.* (2018) – these co-evolving uncertainties projected within a Latin-hypercube sampling results in an overall probability of achieving the target at 66%.

**Paris15C:** Similar to Paris 2C, this scenario aims to limit climate warming to no higher than 1.5˚C global average at 2100. Under the similar Latin-hypercube sampling of structural uncertainties within the Earth and human model systems, this results in a 50% probability of achieving the climate target (i.e. 200 of the 400-member ensemble meets the target).

While these scenarios result in distinct trajectories of global averaged changes in surface-air temperature, most of these distinctions aren't evident until the latter half of the century (**Fig. 3**). Nevertheless, the mid-century impact of the more aggressive climate-based targets (i.e. 15C and 2C scenarios) can be distinguished by the majority of their trajectories of outcomes falling outside the envelope of the BASECOV scenario's trajectories and more so for the 15C scenario. The PFCOV scenario, which captures the current global commitments to reduce emissions (under the Paris Agreement), shows considerable overlap with the BASECOV trajectories by mid-century, yet there is a discernable overall shift toward lower temperatures. Given all these considerations, we gauge the extent of how these global results translate into regional features of risk through a procedure described in the next section.

### 2.3 Regional Climate-Change Pattern Kernels

Climate information from the IGSM is supplied by the MIT Earth Systems Model (MESM) that is able to provide projections of human-forced change at the zonal level of detail. The most recent version of MESM has been extensively evaluated (Sokolov *et al.*, 2018) and includes diagnoses of key hydro-climatic variables, namely precipitation and surface-air temperature. It's performance against observations at the global and zonal scales is comparable to global climate models from Coupled Model Intercomparison Project Phase 5 (CMIP5, Taylor *et al.*, 2012). As previously mentioned, MESM's climate sensitivity is also bounded and sampled

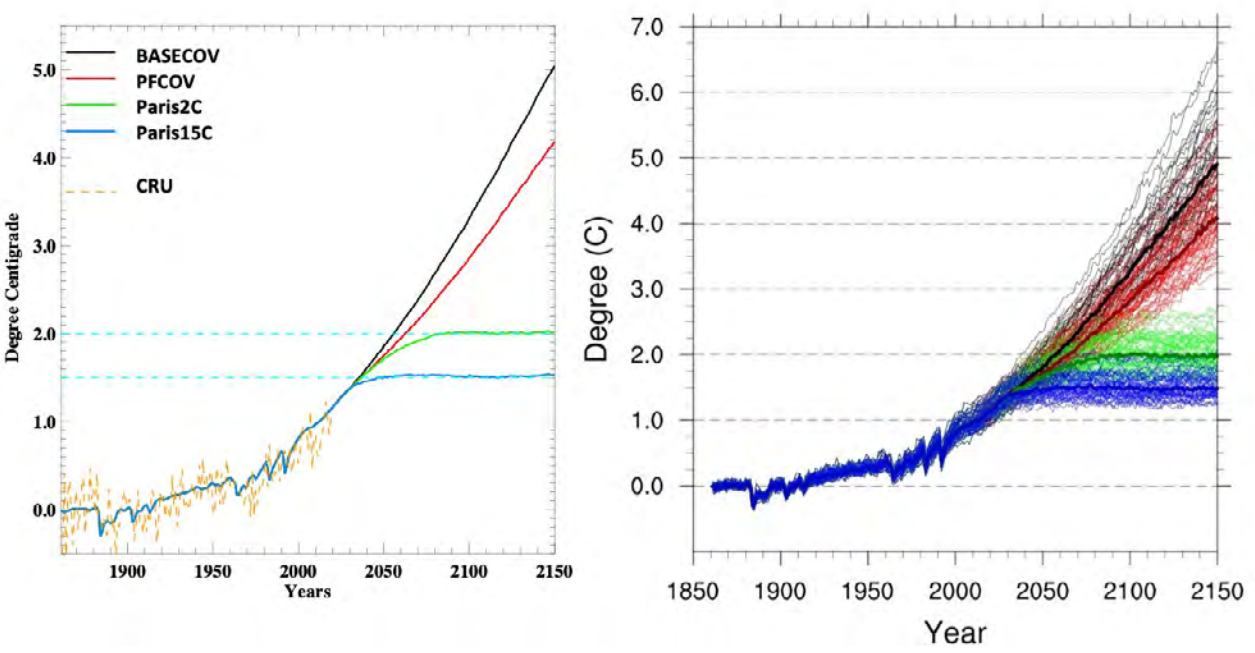


**Figure 3.** Figure adapted from Gao *et al.* (2022, their Figure 2) showing the global averaged annual surface-air temperature trends for the four MIT IGSM scenarios. The left panel presents the median trajectories of the IGSM ensemble, while the right panel provides the trajectories from all ensemble members. Trends in temperature are calculated relative to the 1861-1880 mean provided by the Climate Research Unit (CRU). The colored lines indicate the results from the various scenarios performed by the IGSM and used to construct the hybrid frequency distributions of outcomes (refer to text).

across the range of observed estimates (Libardoni *et al.*, 2018). Further, we have also determined that MESM's global hydrologic sensitivity (i.e. the percent change of global precipitation to a unit increase in global temperature) aligns strongly with state-of-the-art climate models (Paltsev *et al.*, 2021). Thus, MESM is an efficient model that can faithfully produce the global and zonal scale aspects of plausible climate responses to anthropogenic drivers.

To provide regional texture to the MESM simulations, we must expand this information across longitudes using a "pattern scaling" method tailored to the MESM configuration. The use of pattern-scaling methods in climate-change scenario assessments and impact studies is extensive and varied (e.g., Santer *et al.*, 1990; Wigley *et al*, 2000; Mitchell, 2003; Frieler *et al.*, 2012; Lopez *et al.*, 2013; and Herger *et al.*, 2015). For our particular application to the MESM framework, the full description and evaluation is provided in Schlosser *et al.* (2012), and herein we describe the key features of this transformation procedure. In the simplest terms, for any MESM-simulated zonal variable of interest, $V_y$, at a given latitude ($y$) under a human-forced global temperature change ($\Delta T_G$), we can write a transformation of that variable's value at a given longitude ($x$) along the latitude band using the following Taylor-expansion based numerical relationship:

$$V_{x,y}(\Delta T_G) = \overline{C}_{x,y} V_y + \left[\frac{dC_{x,y}}{dT_G}\Delta T_G\right] V_y \qquad (1)$$

where $\overline{C}_{x,y}$ is a climatological-average transformation coefficient, which alters the zonal mean value to a particular value for a longitudinal point along the zonal band. We estimate $\overline{C}_{x,y}$ based on observational data. As discussed in Section 2.1, we will focus our attention on changes in near-surface air temperature ($T_a$) and precipitation. Observational data sources are the same as those used in the prior section that summarized the historical climates for our study region (GPCP and CRU). The projected change in globally averaged temperature, $\Delta T_G$, is relative to a reference or climatological period (1980-1999). The derivative of these transformation coefficients, $\frac{dC_{x,y}}{dT_G}$, for any point $(x,y)$ are discretely estimated from climate model information (for further details, see Schlosser *et al.*, 2012, Section 2 methodology discussion of Equation 4). Therefore, we consider and hereafter refer to the $\frac{dC_{x,y}}{dT_G}$ terms as "pattern-change kernels" (PCKs) of regional climate shifts.

We construct a set of these PCKs from the latest collection of climate/Earth-system models that have participated in the Coupled Model Intercomparison Project Phase 6 (CMIP6, Eyring *et al.*, 2016). The CMIP6 model archive provides a comprehensive set of outputs from climate and Earth-system models that have been developed at institutes across the international scientific community. For the purposes of constructing the PCKs for this analysis, the CMIP6 model archive provides a much larger pool of participating models (29) than the pool of models that were

employed from CMIP5 (18). In some cases, these institutes submitted multiple results that were conducted by their model under a variety of different configurations (e.g., different spatial resolutions and/or various parameterization prescriptions). In constructing this meta-ensemble, we did not incorporate "sibling" model results and instead selected only one set of model results per institute to determine a representative PCK. This was done to avoid biasing in the meta-distribution that would result from using "sibling" PCKs (and thereby inappropriately stacking a regional pattern of change). The CMIP6 models and their configurations chosen for the PCK construction are shown in **Table 2**. As a comparison to prior work conducted (Schlosser *et al.*, 2021), the CMIP5 models that were selected for the PCK construction are provided in **Table 3**. Given the problematic nature of assessing the relative fidelity climate model projections (e.g. Reifen and Toumi, 2009), there was no preferential selection to one model result (e.g. the highest spatial resolution) when multiple configurations were available from an institute. This was also done so as to avoid any other possible sources of biasing when deriving these PCKs across all the models/institutes, and to achieve a diverse sampling of outcomes. The generation Each of the PCKs were constructed at the native model resolution, and then interpolated to a 2˚x2.5˚ common grid, which was commensurate with the coarsest model grid from the

**Table 2**. List of CMIP6 models used in our study to construct the pattern-scaling kernels of climate change response.

| Model Name | Resolution | Institution |
|---|---|---|
| ACCESS-ESM1-5 | 1.875°x1.25° | Australian Commonwealth Scientific and Industrial Research Organization |
| AWI-ESM-1-1-LR | 1.875°x1.875° | German Alfred Wegener Institute |
| BCC-CSM2-MR | 1.125°x1.125° | Beijing Climate Center |
| CAMS | 1.125°x1.125° | Chinese Academy of Meteorological Sciences |
| CanESM5 | 2.8125°x2.8125° | Canadian Centre for Climate Modelling and Analysis |
| CESM2 | 1.25°x0.9375° | National Center for Atmospheric Research |
| CIESM | 1.25°x0.9375° | Department of Earth System Science, Tsinghua University |
| CMCC-ESM2 | 1.25°x0.9375° | Centro Euro-Mediterraneo Cambiamenti Climatici |
| CNRM-ESM2-1 | 1.40625°x1.40625° | Centre National de Recherches Meteorologiques |
| EC-Earth3 | 0.703125°x703125° | EC-Earth-Consortium |
| E3SM | 1°x1° | U.S. Department of Energy |
| FGOALS-g3 | 2.0°x2.25° | Chinese Academy of Sciences |
| FIO-ESM-2-0 | 1.25°x0.9375° | Qingdao National Laboratory for Marine Science and Technology |
| GISS-E2-2-G | 2.5°x2.0° | Goddard Institute for Space Studies |
| HadGEM3-GC31-MM | 0.83°x0.56° | Met Office Hadley Centre |
| IITM | 1.875°x1.91° | Indian Institute of Tropical Meteorology |
| INM-CM5-0 | 2.0°x1.5° | Russian Academy of Science |
| IPSL-CM6A-LR | 2.5°x1.26° | Institut Pierre Simon Laplace |
| KACE | 1.875°x1.25° | Korea Meteorological Administration |
| KIOST | 1.875°x1.875° | Korea Institute of Ocean Science & Technology |
| MCM | 3.75°x2.25° | University of Arizona |
| MIROC-ES2L | 2.8125°x2.8125° | Japan Agency for Marine-Earth Science and Technology |
| MPI-ESM1-2-HR | 0.9375°x0.9375° | Max Planck Institute for Meteorology |
| MRI-ESM2-0 | 1.125°x1.125° | Japan Meteorological Research Institute |
| NorESM2 | 1.25°x0.9375° | Norwegian Climate Consortium |
| SAM0-UNICON | 1.25°x0.9375° | Seoul National University |
| TaiESM2 | 1.25°x0.9375° | Research Center for Environmental Changes, Taiwan |
| UKESM1-0-LL | 1.875°x1.25° | Met Office Hadley Centre |

**Table 3.** List of CMIP5 models used to construct the pattern-scaling kernels of climate change response. Shown are the model acronyms, institute/model name, and the horizontal spatial resolution of the model's output used.

| Model Name | Resolution | Institution |
|---|---|---|
| ACCESS1-3 | 1.875˚ x 1.25˚ | Australian Community Climate and Earth-System Simulator |
| BCC-CSM1-1-m | 1.125 ˚ x 1.125˚ | Beijing Climate Center |
| BNU-ESM1 | 2.8125˚ x 2.8125˚ | Beijing Normal University |
| CanESM2 | 2.8125˚ x 2.8125˚ | Canadian Earth-System Model |
| CESM1-BGC | 1.25˚ x 0.9375˚ | Community Earth System Model (NCAR) |
| CMCC-CM | 0.75˚ x 0.75˚ | Centro Euro-Mediterraneo Cambiamenti Climatici Climate Model |
| CNRM-CM5 | 1.40625˚ x 1.45˚ | Centre National de Recherches Meteorologiques |
| CSIRO-Mk3-6-0 | 1.875˚ x 1.875˚ | Commonwealth Scientific and Industrial Research Organization |
| FGOALS-s2 | 2.8125˚ x 1.66˚ | Flexible Global Ocean-Atmosphere-Land System |
| GFDL-CM3 | 2.5˚ x 2.0˚ | Geophysical Fluid Dynamics Laboratory |
| GISS-E2-R | 2.5˚ x 2.0˚ | Goddard Institute for Space Studies |
| HadGEM2-ES | 1.875˚ x 1.25˚ | Hadley Centre Global Environmental Model |
| INMCM4 | 2.0˚ x 1.5˚ | Institute of Numerical Mathematics |
| IPSL-CM5B-LR | 3.75˚ x 1.875˚ | L'institut Pierre-Simon Laplace Coupled Model |
| MIROC5 | 1.40625˚ x 1.40625˚ | Model for Interdisciplinary Research on Climate |
| MPI-ESM-MR | 2.5 x 1.25˚ | Max Planck Institute |
| MRI-CGCM3 | 1.125 x 1.125˚ | Meteorological Research Institute |
| NorESM1-M | 2.5 x 1.875˚ | Norwegian Earth System Model |

CMIP6 model pool. Further, we construct the (29) PCKs using the results from the 1% transient $CO_2$ simulations. Combined with the 400 members of a MESM ensemble (at a 4˚ zonal resolution), we employ (1) to obtain patterns of change results in a meta-ensemble of 11,600 members per scenario (described in Section 2.2). This 11,600-member meta-ensemble we refer to as a "hybrid frequency distribution" (HFD). Each HFD is used as the basis of our risk quantification and represents the range of outcomes that results from the global and regional structural uncertainties (from MESM and the PCKs). As a precursory assessment, we summarize the model-mean, consensus and diversity of the PCKs across the CMIP6 models – and we also provide a comparison to the PCKs that have been obtained in prior work (e.g., Schlosser *et al.*, 2021) using the CMIP5 models.

### 2.3.1 Temperature

Overall, the multi-model means of $\frac{dC_{x,y}}{dT_G}$ (or PCK) for $T_a$ (**Fig. 4**) exhibits a distinct "colder ocean and warmer land" (COWL) pattern (e.g. Broccoli *et al.*, 1998) across all seasons. The most notable feature in the seasonality of the PCKs is that the extent of the relative maxima across the southern and northern flanks of Africa vary, with the strongest extent occurring in JJA (June-August) and the weakest during DJF (Dec-Feb). Regionally speaking, the strongest degree of seasonality in these features is seen over the EAfr region. As described in the prior section, the effect of this PCK is to then produce an enhanced warming over land as global (and zonal) temperatures rise – as predicted and provided by MESM. This enhanced warming is at its greatest spatial extent across Africa during JJA, and at its weakest during summer (DJF). While the multi-model mean (MMM) of the PCKs suggest that this enhanced warming is consistent across all land areas, a closer inspection of the individual model PCKs (**Fig. 5**) multiple model results shown for DJF) indicates there distinct exceptions - and some cases reversal – to this enhanced warming. In several cases, this opposing *relative* trend covers portions of the Congo region or large regions across eastern and northern Africa, and other features show isolated buffered/reversed relative warming patterns to warming that are confined to a shallow inland extent from a coastline.

In terms of the consistency in the multi-model mean PCKs between CMIP6 and CMIP5, the overall patterns show a strong consistency (**Fig. 6 and Table 4**). The spatial correlations between the MMM CMIP6 and CMIP5 PCKs are very strong across all seasons (obtaining values of at least 0.97).

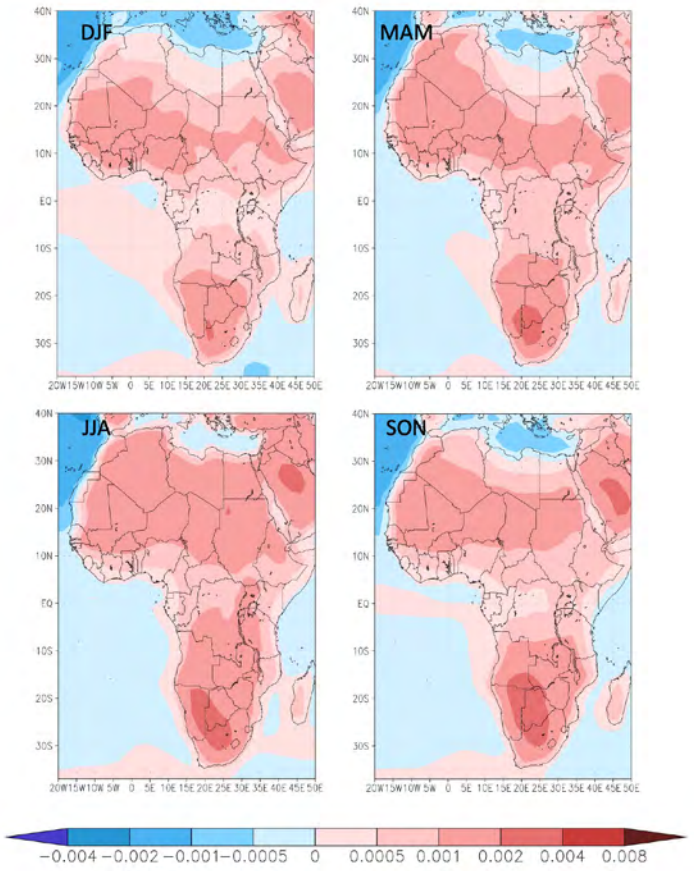


**Figure 4.** Maps of the pattern-change kernel (PCK) coefficients, dCx,y /dTglobal (units of K-1), over Africa for surface-air temperature averaged over the results from the CMIP6 climate models. Shown are the seasonally averaged pattern shifts for: December-February (DJF), March-May (MAM), June-August (JJA), and September-November (SON).

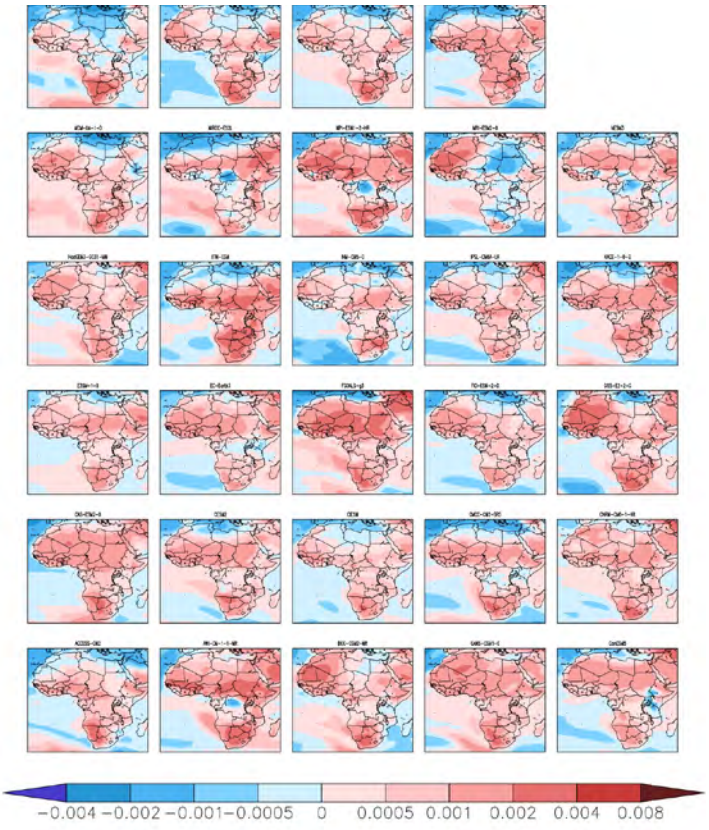


**Figure 5.** Maps of the pattern-change kernels (PCKs) coefficients, dCx,y /dTglobal (units of K-1),, over southern Africa for surface-air temperature. Shown are the results for each model of the CMIP6 collection of the seasonally averaged pattern shifts for December-February (DJF).

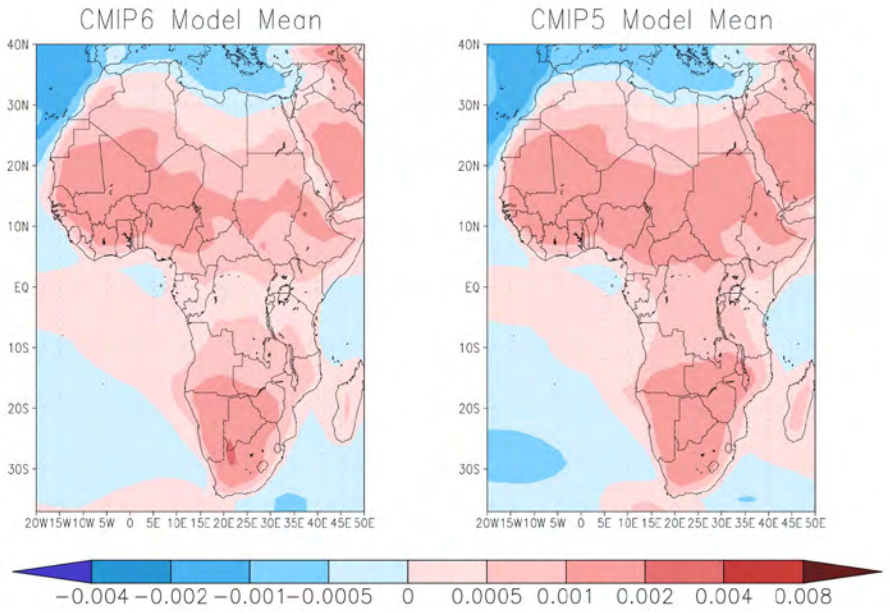


**Figure 6.** Comparison of the DJF averaged PCKs for surface-air temperature obtained from the CMIP6 models (left panel) and the CMIP5 models. Each map depicts the mean of all the individual PCKs obtained from each of the CMIP6 models (29) and the CMIP5 models (18).

### 2.3.2 Precipitation

The MMM as well as inter-model features of the PCKs for precipitation (**Fig. 7**) show a greater degree of heterogeneity (as compared to temperature) across all seasons and regions. However, the most persistent feature is the PCKs imposing a relatively weaker precipitation rate as climate warms across much of the SAfr region for all seasons. In contrast, regions in which the model-mean PCK would impart the strongest relative precipitation rate enhancement (as climate warms) occur at 10˚N during MAM (March-May) and 10˚S during DJF. Across equatorial Africa, a strong relative drying would be imposed by the PCKs during MAM, and during the JJA and SON (Sept.-Nov.) seasons the PCK "splits" into a drying pattern to the north and wetting pattern to the south of the equator. Overall, the most widespread PCK patterns occur during the MAM and SON seasonal periods. Yet the strongest enhanced precipitation trend is seen across 10˚S during DJF. Notwithstanding these common features in the model-mean results, the prominent feature to the precipitation PCKs (particularly in light of the temperature PCKs) lies in the explicit inter-model features.

Looking at the PCKs across the individual models (**Fig. 8**) provides the results for DJF as an example), there are subsets of models that present qualitatively similar large-scale orientations of relative increases and decreases compared to the MMM patterns. However, each model PCK carries with it unique, and in some cases opposing, features that are commensurate in spatial scale to the Africa sub-regions of interest. The most notable example is seen over the SAfr region. While the majority of the PCKs from the CMIP6 models convey a drying trend over large portions of the SAfr region (consistent with the MMM result), there are a subset of models that are in stark and opposing contrast to this – with wetting trends across much of the SAfr region. This highlights the strength of this approach in its ability to efficiently track these unique features and explicitly account for them in the resultant HFD projections. Another example of this type of opposing behavior can be seen over the WCA region, with a PCK from one CMIP6 model producing a large wetting pattern, while another produces a large drying pattern, and yet the MMM pattern exhibits a relatively weak pattern – and consistent with the two opposing PCK patterns offsetting one another. This also highlights a caveat in the use and interpretations made with multi-model averages – particularly for the case of assessing and quantifying risk – as strong signals from individual results are smoothed out and lost in the overall interpretation.

**Table 4.** Spatial correlations between the pattern-change kernels (PCKs) obtained from the CMIP6 collection of models compared to those from the CMIP5 models. For each correlation, a multi-model mean of all the PCKs is taken first (29 patterns from CMIP6 and 18 patterns from CMIP5), and then their seasonal means are calculated: DJF (Dec-Feb), MAM (March-May), JJA (June-Aug), and SON (Sept-Nov). The spatial correlations shown are for the seasonally averaged, multi-model mean PCKs for precipitation (PCP) and surface-air temperature (T).

| | $PCK_{PCP}$ | $PCK_{T}$ |
|---|---|---|
| **DJF** | 0.43 | 0.97 |
| **MAM** | 0.58 | 0.98 |
| **JJA** | 0.74 | 0.99 |
| **SON** | 0.78 | 0.98 |

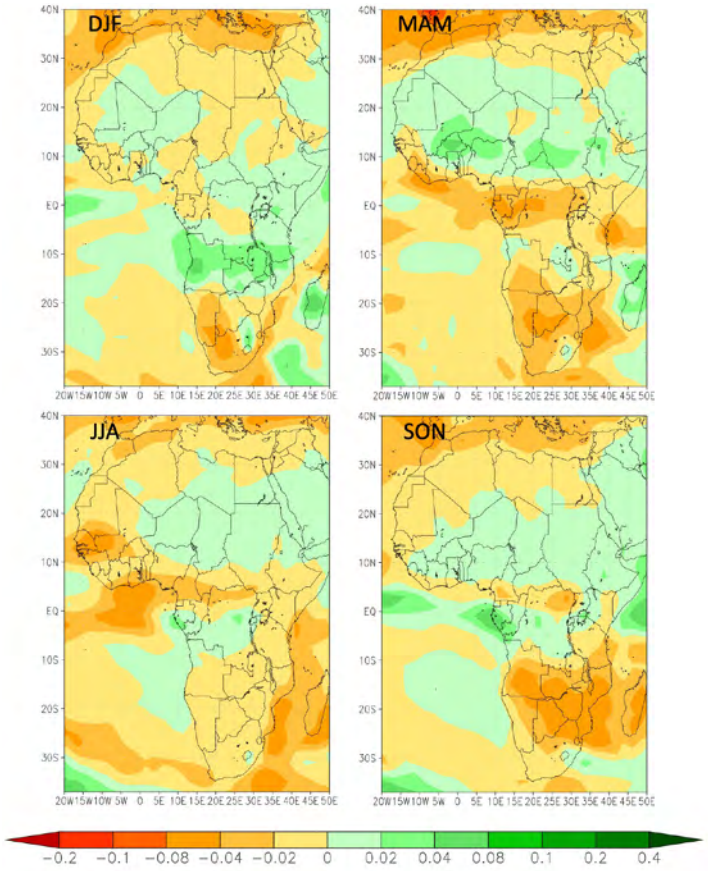


**Figure 7.** Maps of southern Africa showing the pattern-change kernel (PCK) coefficients, dCx,y /dTglobal (units of K-1), for precipitation averaged over the results from the CMIP6 climate models. Seasonally averaged pattern shifts shown for: December-February (DJF), March-May (MAM), June-August (JJA), and September-November (SON).

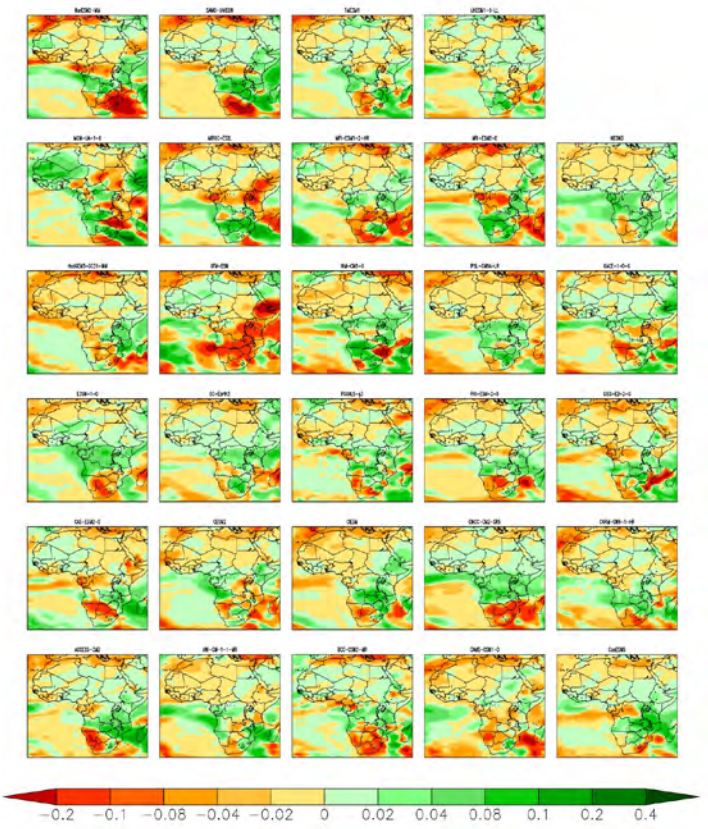


**Figure 8.** Maps of southern Africa from each model of the CMIP6 collection showing pattern-change kernel (PCK) coefficients, dCx,y /dTglobal (units of K-1), for seasonally averaged precipitation pattern shifts for December-February (DJF)

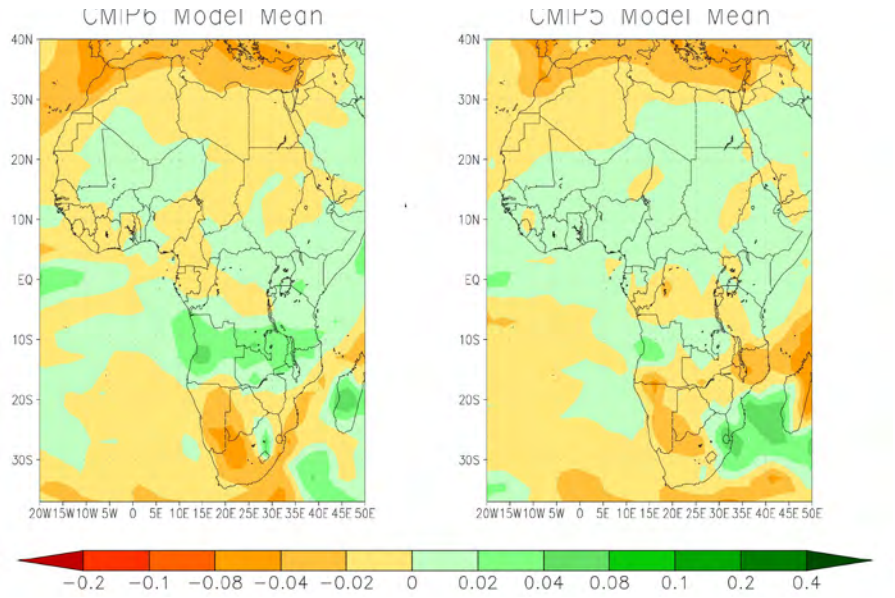


**Figure 9**. Comparison of the DJF averaged PCKs for precipitation obtained from the CMIP6 models (left panel) and the CMIP5 models. Each map depicts the mean of all the individual PCKs obtained from each of the CMIP6 models (29) and the CMIP5 models (18).

Perhaps consistent with these specific features across the precipitation PCKs for the individual CMIP6 models, the consistency of the MMM features to those derived from the CMIP5 models is, overall, weaker than that seen for temperature across all seasons (Table 4). In addition, the consistency for the precipitation PCKs has a distinct seasonality with the strongest consistency during the SON and JJA seasonal periods, and weakest during the DJF and MAM seasonal periods. Taking a closer look at the DJF seasonal period (**Fig. 9**), the most notable distinctions that contribute to the reduced consistency are seen in the strong wetting trend in the CMIP6 pattern at 10˚S (much weaker if not absent in CMIP5), opposing trends across much of the Nile River basin, as well as contrasting features across much of South Africa and Madagascar.

In light of all these considerations, the resultant HFD distributions will be explored across the large Africa sub-regions (i.e., EAfr, WCA, and SAfr) in the section that follows. The analyses will consider the general time-evolving nature of the median, interquartile, and extremes of the projections' populations, and contrast each scenario for each region. A closer inspection of the distribution of outcomes will then be presented for specific times and scenarios to highlight the impact of the stronger mitigation on the implied hydroclimatic risks across the sub-regions.

## 2.4 Hybrid Frequency Distribution (HFD) Results

### 2.4.1 Timeseries of Changes

For all the sub-regions considered, there is a strong consistency in the surface-air temperature responses compared across the scenarios out to 2040 (**Figs. 10-12**) and is particularly evident in the median results from the HFD populations. However, by mid-century, the impact of reduced warming from the mitigation efforts in the Paris15C scenario is distinct from the others and persists for the remainder of the projections. It is not until the final decade of the simulation period (the 2060s) that the median results from each scenario show a discernable trajectory. However, in terms of other key features in the distribution of outcomes (lower panels of Figs. 10-12), the Paris2C and Paris15C trajectories share a concave down characteristic feature, whereas the BASECOV and PFCOV trajectories exhibit slightly concave up tendencies.

In contrast, the results for precipitation (**Figs. 13-15**) display more distinct behaviors across the sub-regions, and this is owing in large part to the more distinct features in the PCKs that were constructed (shown in section 2.3.2). The most notable distinction is that for the SAfr region, the preponderance of the trajectories indicates reduced precipitation over the region due to human-forced climate warming. Nevertheless, the median results between all the regions still share a common response across the scenarios like that seen for surface-air temperature, in that the trajectory of the Paris15C is most clearly distinct from the others until mid-century. While these features demonstrate the important impact of strong mitigation on the median and other key features in the distribution of outcomes, in the analysis that follows, a closer inspection of the distributions are presented to highlight hydroclimatic risk implications.

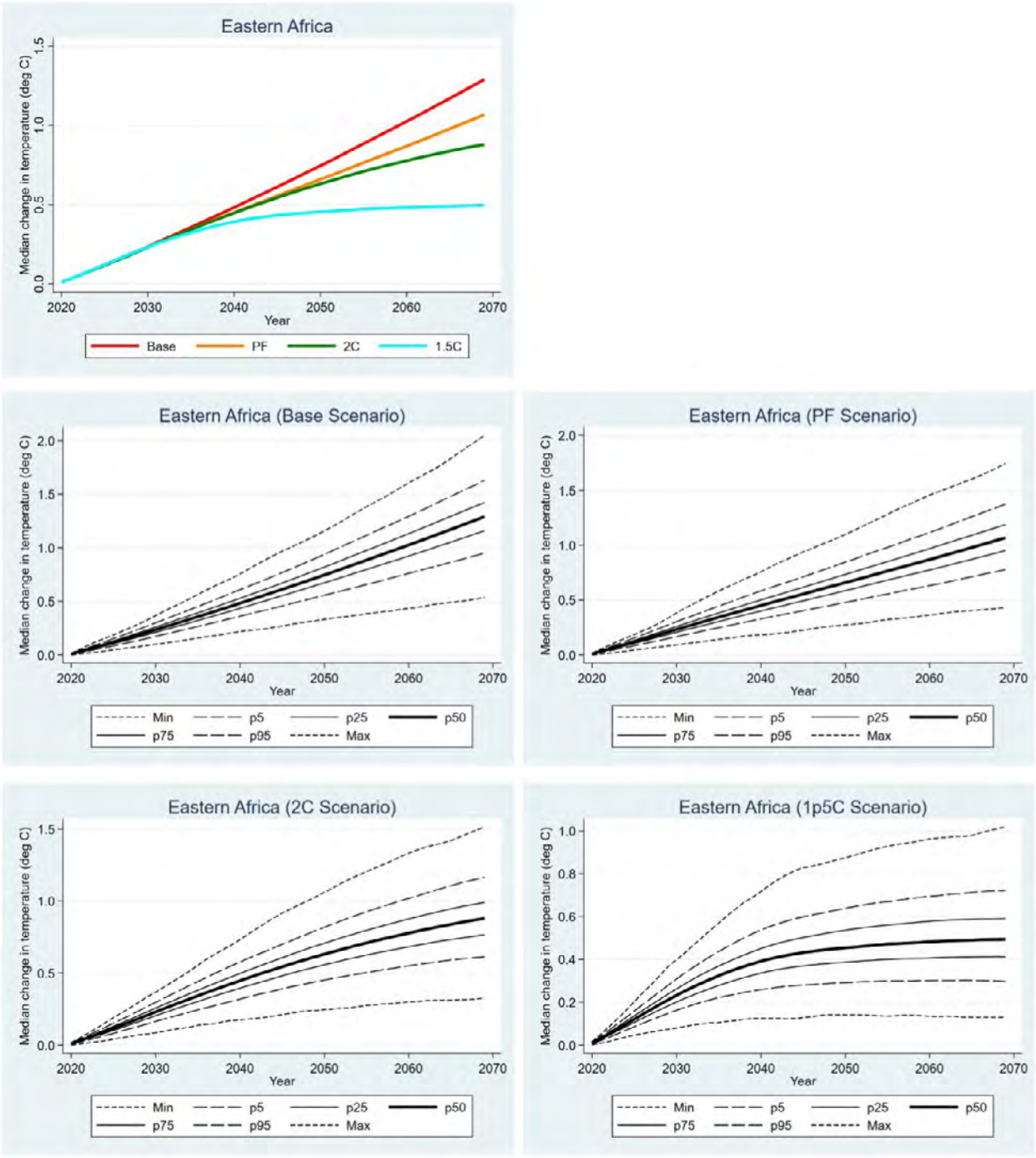


**Figure 10.** Timeseries of key statistical features for annual surface-air temperature change (units in ˚C) obtained from the hybrid frequency distribution (HFD) scenarios, averaged for the Eastern Africa (EAfr) region. The surface-air temperature change is based against the 2000-2019 average and represents a 20-year smoothed result. In the top panel, the median outcome of the HFDs for each of the IGSM scenarios is presented (and scenario results color coded). In the bottom panels, the key statistical features of the HFD outcomes are presented: short-dash lines are min/max; long-dash lines are 5$^{th}$ and 95$^{th}$ percentile values; thin-solid lins are the lower/upper quartile values; and thick solid lines are the median values. Each of the lower panels presents the results for the BASECOV ("Base Scenario"); PFCOV ("PF Scenario"); Paris2C ("2C Scenario"); and Paris15C ("1p5C Scenario") scenarios.

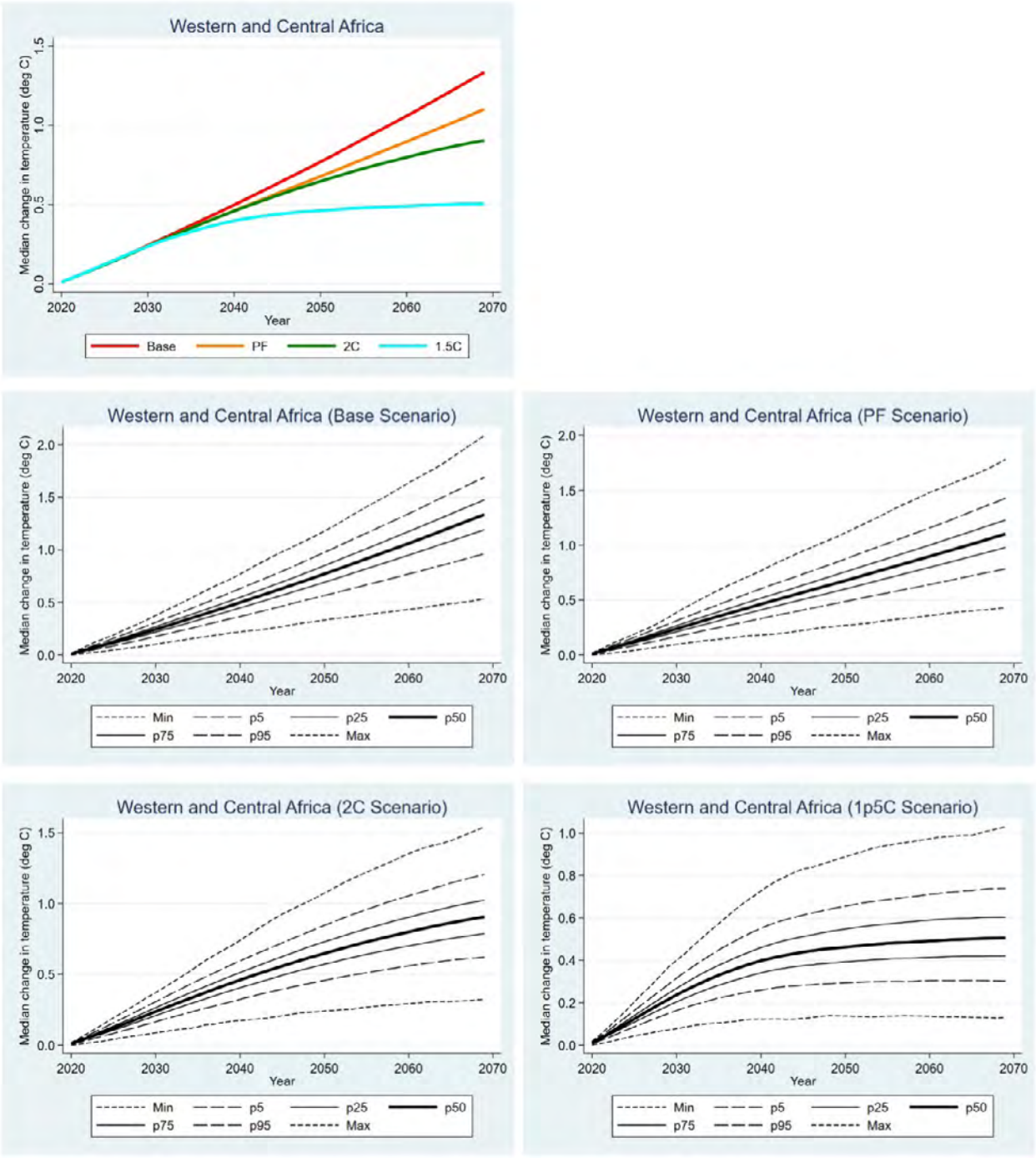


**Figure 11.** As in Fig. 10, but for the results averaged over the western and central Africa (WCA) region.

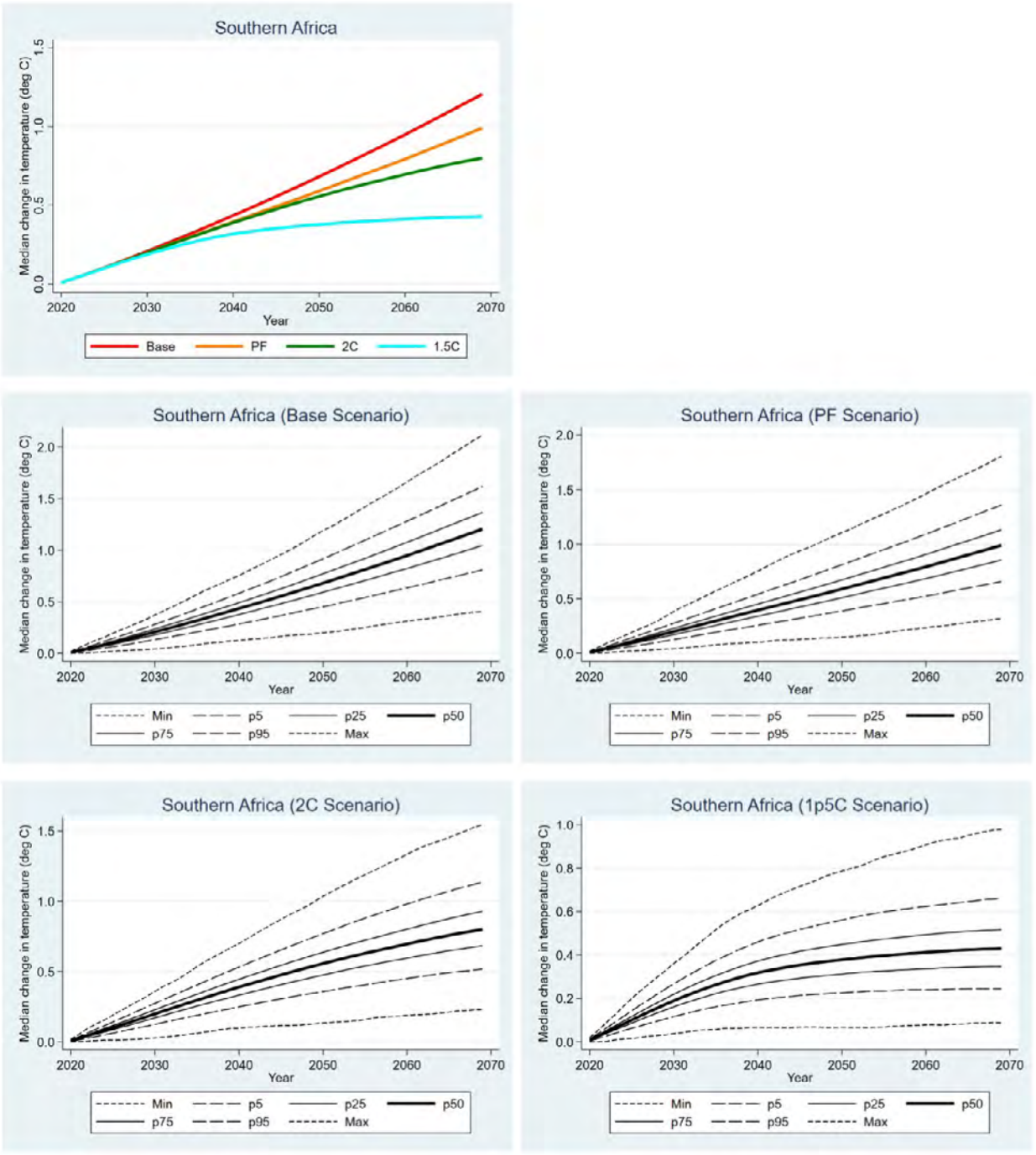


**Figure 12.** As in Fig. 10, but for the results averaged over the southern Africa (SAfr) region.

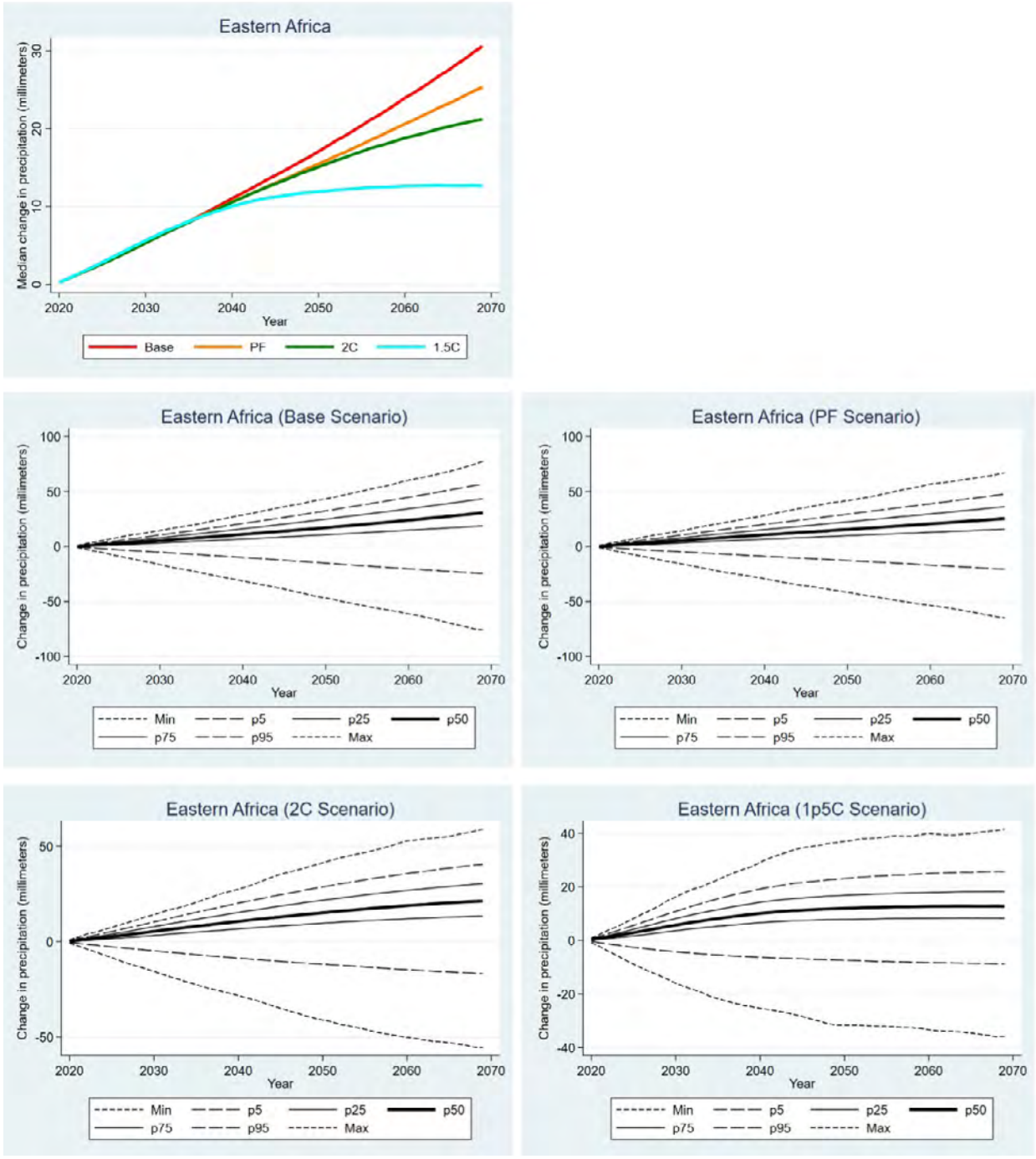


**Figure 13.** As in Fig. 10, but for changes in annual precipitation (units in mm/year), averaged over the Eastern Africa (EAfr) region.

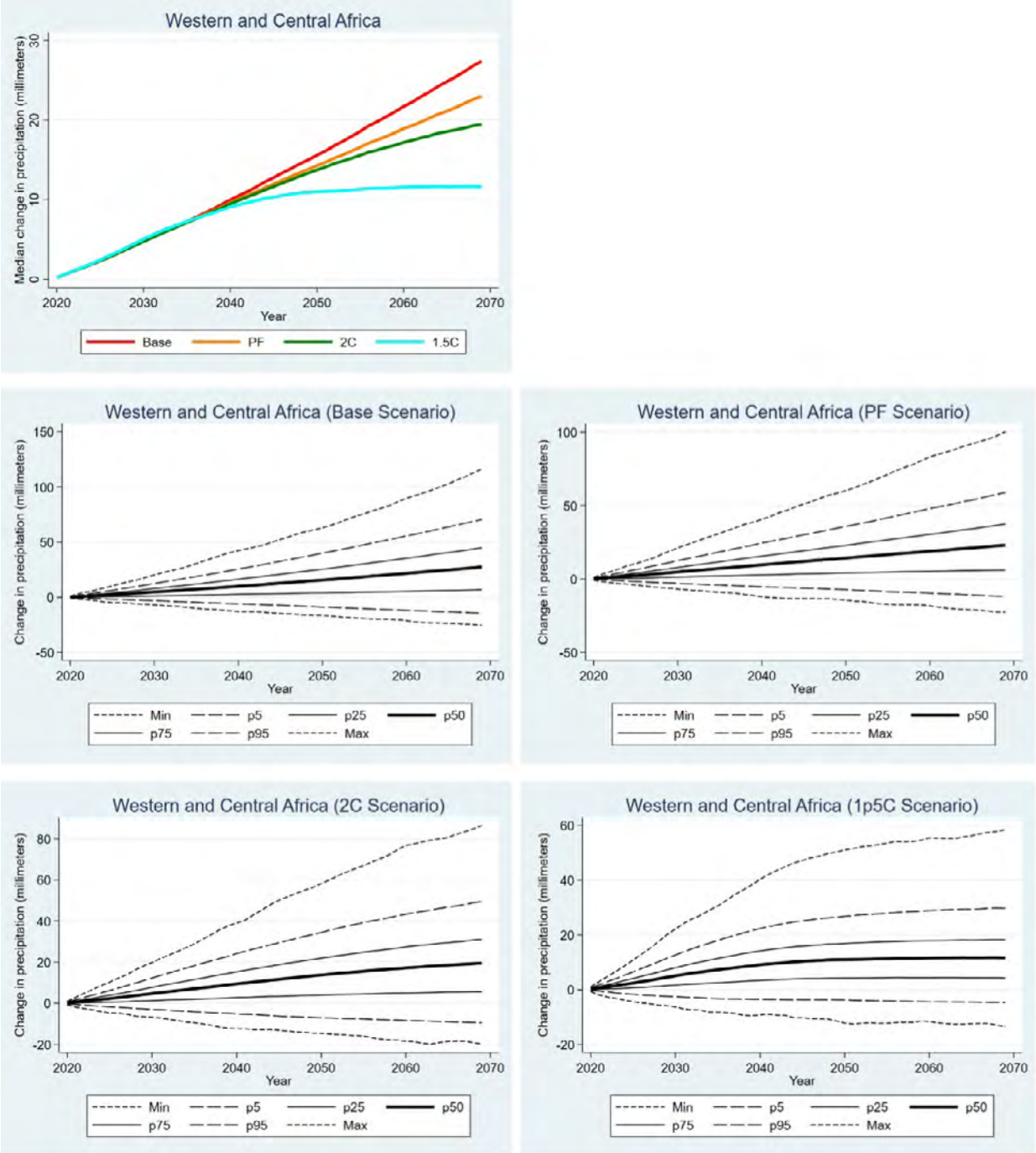


**Figure 14.** As in Fig. 13, but for the results averaged over the western and central Africa (WCA) region.

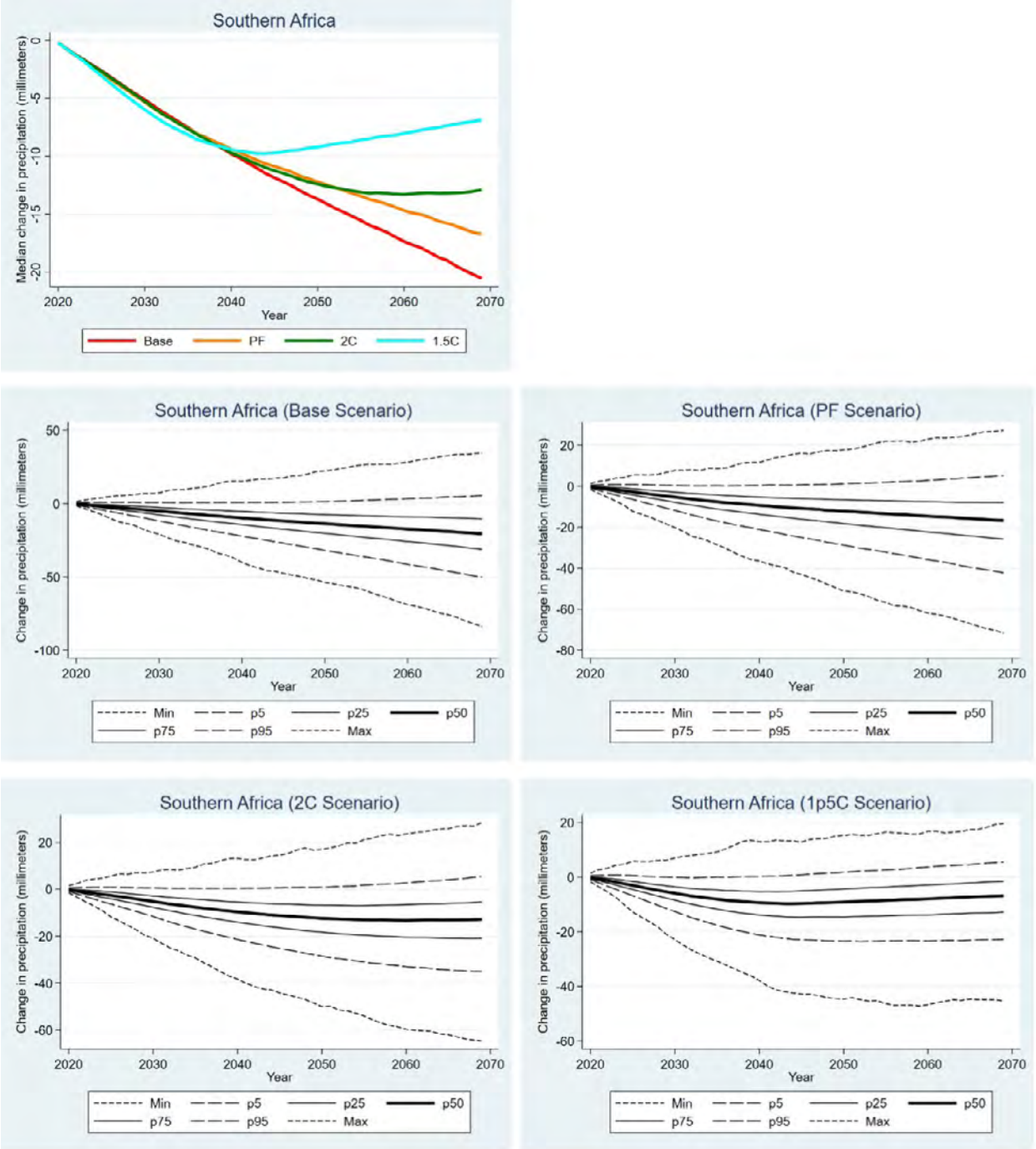


**Figure 15.** As in Fig. 10, but for the results averaged over the southern Africa (SAfr) region.

### 2.4.2 Mid-Century Distributional Changes

For all the regions considered through the mid-century, there is a virtual certainty that seasonally-averaged surface-air temperatures will warm to a level that is "salient" relative to historical variations (**Figs. 16 and 17**). The notable exception to this characterization is seen over the SAfr for the DJF seasonal period and indicates that the strongest mitigation pathway (Paris15C) would provide a roughly 1-in-3 chance that any warming would be below what could be regarded as salient. As previously discussed (in Section 2.1), the threshold of salience is judged against observed climatological variability (Table 1), and we set a value of 2 standard deviations to the seasonally-averaged decadal-mean quantities (indicated by the blue shaded bin region) – at or beyond which any change is regarded as "salient". In the strict sense, this is not an indication of statistical significance but when considering any variable that is aligned with a Gaussian distribution (such as surface-air temperature) the ±2 standard deviation range would span 95% of the total population of values. Therefore, by this measure, a temperature change of this magnitude (and higher) directly associated with anthropogenic emissions lies among the severe-to-extreme climatological population of decadal variation.

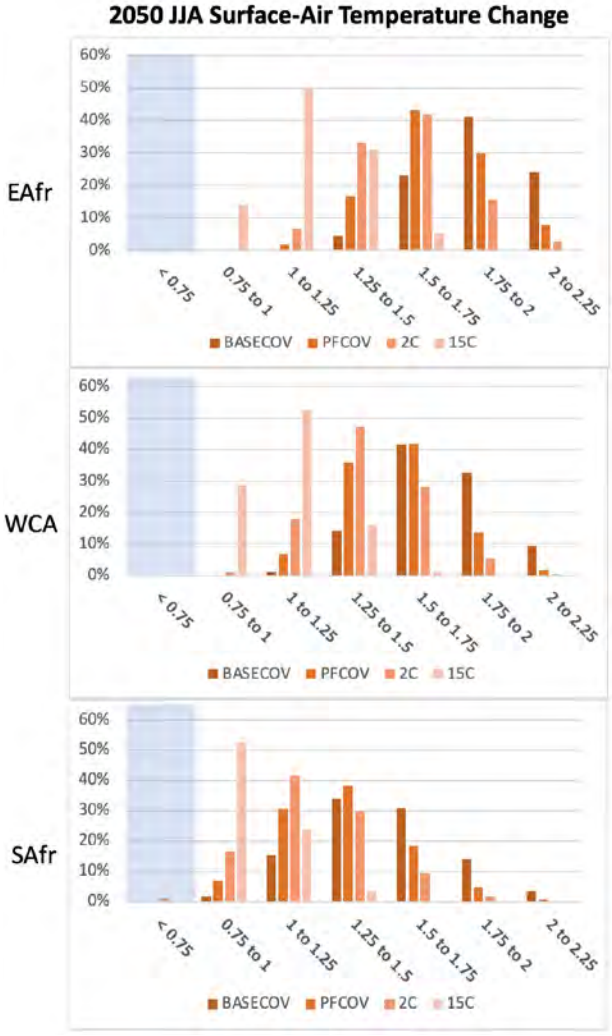


**Figure 16.** Hybrid frequency distributions (HFDs) of decadal- and area-averaged surface-air temperature change (˚C) for 2050-2059 relative to the last decade of the 20th century in all three sub-regions of Africa (EAfr, WCA, and SAfr) averaged for June-August (JJA). Each panel provides results for all four IGSM scenarios (refer to text for details). The binned area shaded in blue represents the temperature change that falls within the two-standard deviation of historical decadal variability (as depicted in Fig. 2 and Table 1).

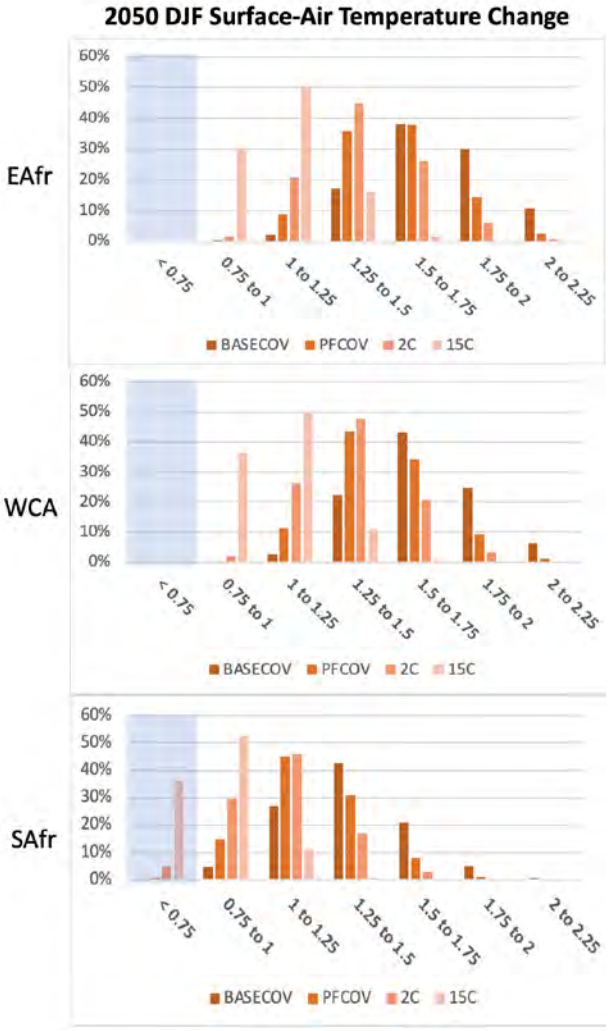


**Figure 17.** As in Fig. 16, but for the HFDs of surface-air temperature change averaged over DJF (Dec-Feb).

In view of this, the results from the HFDs indicate that in all futures considered except the 15C scenario, over 95% of the total population of outcomes result in temperature changes above the level of salience (Figs. 16 and 17, all panels). Most notably, for the EAfr region for all seasons (only DJF and JJA seasonal periods shown), the BASECOV, PFCOV, and Paris2C scenarios show that at least 50% of their distributions result in temperature changes that are double in magnitude to the salience threshold (a 1.5˚C warming or higher). These likelihoods are substantially reduced in the Paris15C scenario, with less than 10% of the distribution at the commensurate level of warming. Similar results are seen for the WCA region, with the main distinction that Paris2C mitigation has a stronger benefit and keeps the higher probability of warming below the doubling from the salience threshold. In all seasonal periods and regions, the impact of the Paris15C at reducing the likelihood of warming well above the salience threshold (i.e. doubling) is clear, with as much as 80% of the distribution residing in warming below that level.

As previously noted (Section 2.3.2), the precipitation pattern-changes across the CMIP5 models differ in sign and structure both across and within the sub-regions of interest. Therefore, the resultant HFDs will (necessarily) reflect likelihoods of both increased and decreased change. Similar to precipitation, we prescribe a degree of salience in order to provide a quantitative judgement on the magnitude of change. Additionally, the relative preponderance of "salient" changes toward drier or wetter precipitation rates is also gauged under the recognition that equal chances of a dry or wet future would be the equivalent to a proverbial "coin-toss" as to how one should view the risk of change. Under these considerations, the expected changes in precipitation by mid-century (**Fig. 18**) and indicate that there is a greater risk of a "salient" increase in precipitation for the EAfr and WCA regions and a greater risk of decrease over the SAfr region. In the BASECOV scenario by mid-century, the portion of the distribution with decreased DJF precipitation change for SAfr is 15 times that of increased precipitation (15% versus 1%). A similar contrast in outcomes is seen for the EAfr region, but the preponderance toward increased precipitation. For the WCA region, there are no outcomes in which a decrease in precipitation exceeds the salience threshold, but approximately 20% of the BASECOV population of outcomes exceeds the increased precipitation threshold. For all these basins, these characteristic preponderances are largely maintained in the PFCOV and Paris2C scenarios (at mid-century).

### 2.4.3 The Evolution of Risk and Impact of Climate Targets to Abatement

As we have shown for these changes hydroclimatic risks, there is a very clear impact of the more aggressive climate target scenario at reducing (and nearly eliminating) the risk of the very salient (as given by our metrics) temperature

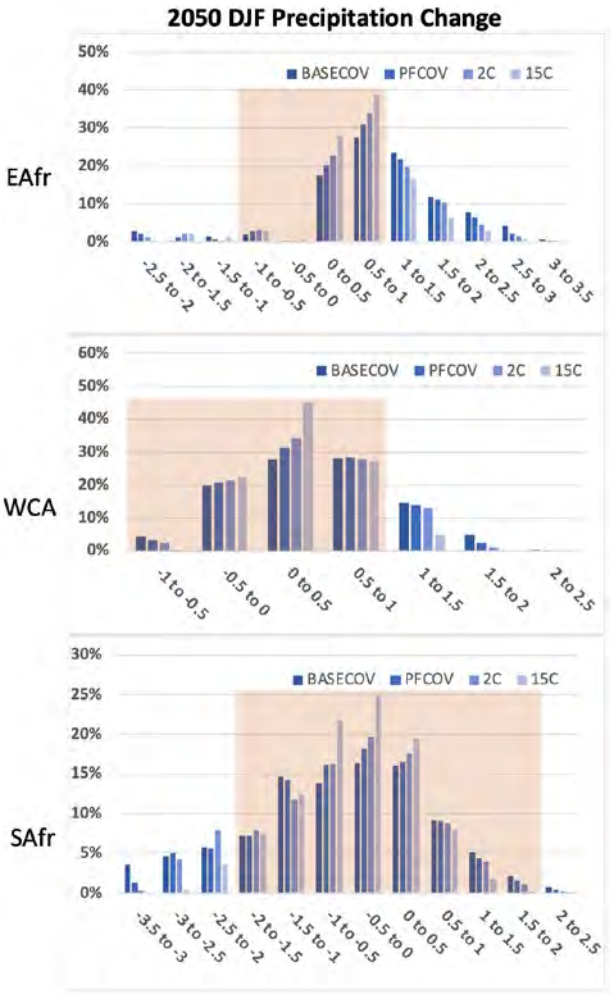


**Figure 18.** As in Fig. 17, but for the HFDs of precipitation change. Units are given in mm/decad (decad = 10 days). The red shaded areas represent the precipitation change that falls within the two-standard deviation of historical decadal variability (as depicted in Fig. 2 and Table 1).

changes. Stemming from the diversity in the modeled precipitation response patterns (Section 2.3), and that precipitation change is not a positive definite change process as the case for temperature, the impacts of climate-target scenarios reducing risks in precipitation change exhibit different characteristics in their behavior. Whether considering the time trajectories (e.g., Figs. 10-15) or scenario-dependent distributional behaviors (e.g., Figs. 16-18), the HFDs of primarily respond by broadening and/or tightening of the range of outcomes, and as previously noted, for the case of precipitation the relative preponderance toward positive or negative change is altered. Consistent to this behavior is the substantial portion of the distribution still contained within the range of changes that are not regarded as "salient" (within the construct of our analyses). This is quite consistent with the variety and diversity of landscapes in the strength and sign of the precipitation PCKs (Section 2.3) across and within the three regions of focus.

Nevertheless, as climate continues to warm, the patterns continue to emerge (at varying rates) and will affect these area-averaged results, and ultimately, unless the warming is reversed (or stopped) "unavoidable" salient changes will emerge. Nevertheless, looking into the latter half of the 21st century (**Figs. 19-22**), the impact of the more aggressive climate targets to reducing the evolving risks, particularly from the BASECOV, scenario becomes evident.

In particular, for surface-air temperature, a notable demonstration in the effectiveness of a strong mitigation scenario (i.e. Paris15C) is made. For all regions and seasonal periods considered (Figs. 19 and 20 show the JJA and DJF results, respectively), the distribution of outcomes in the Paris15C scenario in 2065 are all skewed toward lower "risk" (higher probabilities for lower warming rates) as judged against the BASECOV results for 2035. In particular, for SAfr nearly 35% of the distribution for the DJF seasonal period still resides inside the salience threshold of warming at 2065 for the Paris15C scenario. Equivalently, it indicates that there is a 1-in-3 chance that any warming experienced over


**Figure 19.** HFDs of decadal- and area-averaged surface-air temperature change (units in ˚C) relative to the last decade of the 20th century in all three sub-regions of Africa (EAfr, WCA, and SAfr), averaged for June-August (JJA). Each panel compares changes in two scenarios and different decadal periods: the BASECOV scenario for 2030-2039 and the Paris15C scenario for 2060-2069. The binned area shaded in blue represents the temperature change that falls within the two-standard deviation of historical decadal variability (as depicted in Fig. 2 and Table 1).


**Figure 20.** As in Fig. 19, but for the results averaged over DJF (Dec-Feb).

the region in DJF (summertime) during the latter half of the century would fall within the envelope of natural variability. Similar "risk reductions" can be seen in the results for precipitation (Figs. 21 and 22 show the JJA and DJF results, respectively). For all regions and in both summer and winter, the HFDs of precipitation change between the REF scenario in the 2030s compared to the 15C scenario in the 2065-2074 period are nearly identical, and in most cases the likelihood of precipitation changes that aren't considered salient are more likely in the 15C scenario.

Among other notable impact in the mitigation scenarios are seen across the strongest changes in precipitation. In particular, for the EAfr and SAfr regions, the likelihood of the strongest changes in precipitation changes in 2035 for the BASECOV approaches are double to what the likelihood of these changes would be in 2065 for the Paris15C scenario. This underscores the beneficial aspect of the 15C scenarios, in that the overall risks to precipitation change, are delayed by decades.

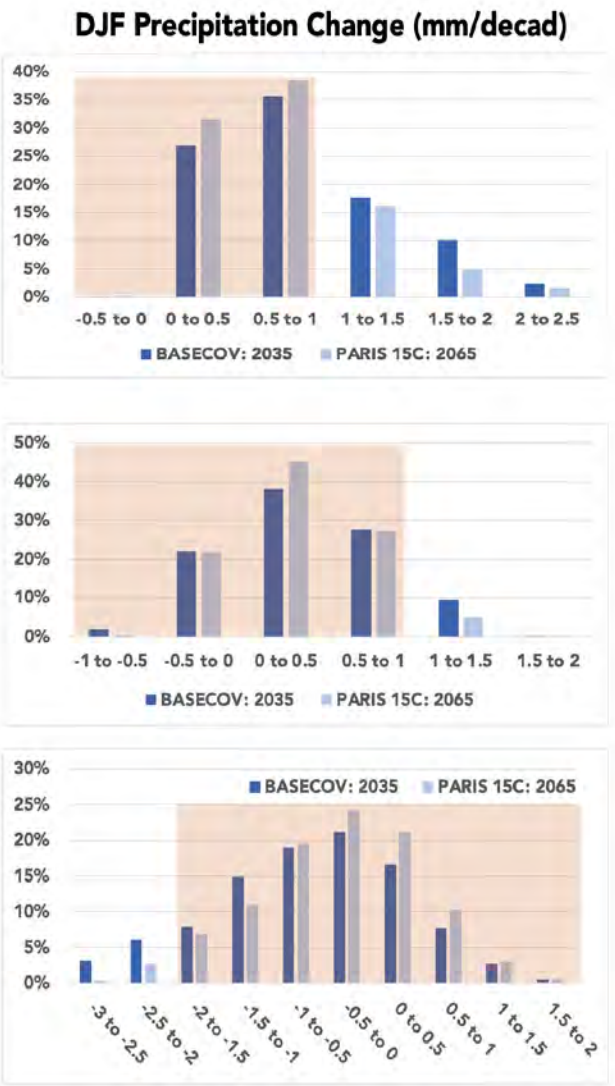


**Figure 21.** HFDs of decadal- and area-averaged precipitation change (units in mm/decad; decad = 10 days) relative to the last decade of the 20th century in all three sub-regions of Africa (EAfr, WCA, and SAfr), averaged for DJF (Dec-Feb). Each panel compares changes in two scenarios and different decadal periods: the BASECOV scenario for 2030-2039 and the Paris15C scenario for 2060-2069. The binned areas shaded in red represents the precipitation changes that falls within the two-standard deviation of historical decadal variability (as depicted in Fig. 2 and Table 1).

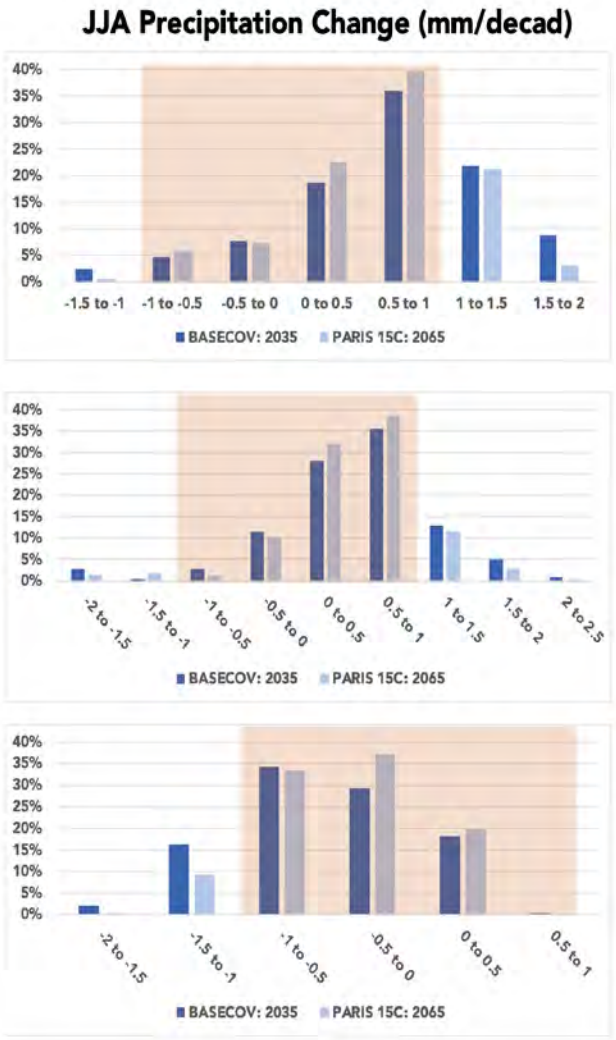


**Figure 22.** As in Fig. 21, but for the precipitation change results averaged over JJA (June-August).

## 3. Summary Remarks

In this study, we have presented risk-based results derived from large ensembles of projected changes in seasonal precipitation and near-surface air temperature over large sub-regions of Africa. The ensemble procedure combines, via a Taylor expansion, regional patterns of emerging climate responses from the CMIP6 climate models with the MIT-IGSM, an intermediate complexity earth-system model coupled to a global economic model that evaluates uncertainty in socio-economic growth, anthropogenic emissions, and global environmental response. Given its computational efficiency, the IGSM can be run for large ensembles (e.g. 400 members in this study) to explore the range of possible global climate responses that result from human and natural forcings. In this study, the numerical experimentation with the IGSM included four scenarios of future climate and socio-economic development in order to span a range of possible global actions to abate greenhouse gas emissions over the coming century. When combined with the CMIP6 regional patterns of climate response (i.e., pattern-change kernels or PCKs), the resultant meta-ensembles (1,000s of members) are used to create "hybrid frequency distributions" (HFDs) in order to examine the evolution of climate and the extent to which global actions can abate or avoid changes that are regarded as hazardous.

We evaluated the HFDs of surface-air temperature and precipitation averaged over three regions across Africa: eastern (EAfr), west central (WCA), and southern (SAfr). Across all these regions, we find that by mid-century unless stronger measures are put into force that set stricter climate targets, summer and winter averaged temperatures will increase (i.e. over 95% of the BASECOV and PFCOV scenario member simulations) "saliently" beyond the current climate's variability. In addition, there is a strong likelihood (in nearly 50% and higher of the BASECOV and PFCOV ensemble scenarios) that by mid-century temperatures will rise considerably higher than the current climate's range of variability (twofold increase over the current climate's two-standard deviation range of variability). More aggressive global climate targets, particularly set in the Paris15C scenario, all but eliminate the risk of these acutely salient temperature increases. For precipitation, the evolving nature of the regional risks exhibits more distinct features across the regions considered. Most notably, across southern Africa, the preponderance of precipitation change across the HFD members indicates that there is a considerably greater likelihood that the region will experience reduced (as opposed to increased) precipitation by mid-century even under current global agreements to reduce emissions. However, without these national commitments (under the Paris Agreement) the likelihood of strong decreases in precipitation (i.e. greater than 2 times the current range of variability) is notable (around 15% of the BASECOV ensemble simulations across all seasonal periods). Given the recent severe drought this region has experienced (e.g. Sousa *et al,* 2018) and the widespread water-efficiency measures put into action to combat the extreme water shortage, the increasing risk of depleted precipitation that these results imply would indicate that such efficiency measures will become more frequently strained and relied upon. Conversely, across the remaining regions of Africa, the distributions of precipitation change indicate a preponderance of increased precipitation.

There is a clear benefit seen within the evolving hydroclimatic risks as a result of strong climate targets, such as limiting the global climate warming to 1.5˚C by 2100 (the Paris15C scenario). In all the regions considered, we find that the risk of precipitation changes in the Paris15C scenario within the latter half of this century (centered at 2065) is comparable, and in most cases buffered, to that seen in the BASECOV scenario in 2035. The distributions that result from the 15C scenario toward the end of this century indicate that not all risks of salient changes are removed. Yet, the critical aspect of this outcome is that the strong mitigation scenarios demonstrate the decades of delay in these risks evolving, relative to the trajectory that is more aligned with current actions to reduce emissions. This 30-year delay will be invaluable toward any national efforts that are needed to prepare and adapt to heightened risks.

**Acknowledgments**

This work was funded by the IFPRI Foresight project, with additional support from the Policies, Institutions, and Markets Research Program of the CGIAR. The authors gratefully acknowledge this as well as additional financial support for this work provided by the MIT Joint Program on the Science and Policy of Global Change through a consortium of industrial sponsors and Federal grants. Development of the IGSM applied in this research was supported by the U.S. Department of Energy, Office of Science (DE-FG02-94ER61937); the U.S. Environmental Protection Agency, EPRI, and other U.S. government agencies and a consortium of 40 industrial and foundation sponsors. For a complete list see https://globalchange.mit.edu/sponsors/current.

## 4. References


Adler, R.F., M. Sapiano, G.J. Huffman, J. Wang, G. Gu, D. Bolvin, L. Chiu, U. Schneider, A. Becker, E. Nelkin, P. Xie, R. Ferraro & D.B. Shin (2018). The Global Precipitation Climatology Project (GPCP) Monthly Analysis (New Version 2.3) and a Review of 2017 Global Precipitation. *Atmosphere* **9**(4): 138 (doi:10.3390/atmos9040138).

Arndt, C., J. Kozlitina & P.V. Preckel (2006). Efficient survey sampling of households via Gaussian quadrature. *J Royal Stat Soc: Series C (Applied Statistics)* **55**: 355–364 (doi:10.1111/j.1467-9876.2006.00537.x).

Arndt, C., P. Chinowsky, C. Fant *et al.* (2019). Climate change and developing country growth: the cases of Malawi, Mozambique, and Zambia. *Clim. Change* **154**: 335–349 (doi:10.1007/s10584-019-02428-3).

Broccoli, A.J., N.-C. Lau & M.J. Nath (1998). The cold ocean–warm land pattern: Model simulation and relevance to climate change detection. *J. Climate,* **11**: 2743–2763.

Chen, Y.-H.H., S. Paltsev, J.M. Reilly, J.F. Morris & M.H. Babiker (2016). Long-term economic modeling for climate change assessment. *Econ Model* **52**(Part B): 867–883 (doi:10.1016/j.econmod.2015.10.023).

Eyring, V., S. Bony, G.A. Meehl, C.A. Senior, B. Stevens, R.J. Stouffer & K.E. Taylor (2016). Overview of the Coupled Model Intercomparison Project Phase 6 (CMIP6) experimental design and organization, *Geosci. Model Dev.* **9**: 1937–1958, doi:10.5194/gmd-9-1937-2016.

Fant, C., Y. Gebretsadik, A. McCluskey & K. Strzepek (2015). An uncertainty approach to assessment of climate change impacts on the Zambezi River Basin. *Clim Chang* **130**:35–48

Frieler, K., M. Meinshausen, M. Mengel, N. Braun & W. Hare (2012). A scaling approach to probabilistic assessment of regional climate change, *J. Clim.* **25**(9): 3117–3144, (doi:10.1175/JCLI-D-11-00199.1).

Herger, N., B.M. Sanderson & R. Knutti (2015). Improved pattern scaling approaches for the use in climate impact studies. *Geophys. Res. Lett.* **42** (doi:10.1002/2015GL063569).

Huffman, G.J., R.F. Adler, D.T. Bolvin & G. Gu (2009). Improving the global precipitation record: GPCP Version 2.1. *Geophys. Res. Lett.* **36**: 1–5 (doi:10.1029/2009GL040000).

Jones, P.D., M. New, D.E. Parker, S. Martin & I.G. Rigor (1999). Surface air temperature and its variations over the last 150 years. *Reviews of Geophysics* **37**: 173–199.

Lennard, C., G. Nikulin, A. Dosio & W. Moufouma-Okia (2018). On the need for regional climate information over Africa under varying levels of global warming. *Environ. Res. Lett.* (doi:10.1088/1748-9326/aab37b).

Libardoni, A.G., C.E. Forest, A.P. Sokolov & E. Monier (2018). Estimates of climate system properties incorporating recent climate change. *Advances in Statistical Climatology, Meteorology and Oceanography* **4**(1/2): 19–36 (doi:10.5194/ascmo-4-19-2018).

Lopez, A., E.B. Suckling & L.A. Smith (2013). Robustness of pattern scaled climate change scenarios for adaptation decision support, *Clim. Change* **122**(4), 555–566 (doi:10.1007/s10584-013-1022-y).

Meehl, G.A., C. Covey, T. Delworth, M. Latif, B. McAvaney, J.F.B. Mitchell, R.J. Stouffer & K.E. Taylor (2007). The WCRP CMIP3 multi-model dataset: A new era in climate change research, *Bull. Amer. Met. Soc.* **88**: 1383–1394.

Mitchell, T.D. (2003). Pattern scaling—An examination of the accuracy of the technique for describing future climates, *Clim. Change* **60**(3): 217–242.

Morris, J. J. Reilly, S. Paltsev, A. Sokolov & K. Cox (2022). Representing socio-economic uncertainty in human system models. *Earth's Future* **10**(4) (doi: 10.1029/2021EF002239).

Niang, I., O.C. Ruppel, M.A. Abdrabo, A. Essel, C. Lennard, J. Padgham & P. Urquhart (2014). Africa. In: *Climate Change 2014: Impacts, Adaptation, and Vulnerability. Part B: Regional Aspects. Contribution of Working Group II to the Fifth Assessment Report of the Intergovernmental Panel on Climate Change* [Barros, V.R., C.B. Field, D.J. Dokken, M.D. Mastrandrea, K.J. Mach, T.E. Bilir, M. Chatterjee, K.L. Ebi, Y.O. Estrada, R.C. Genova, B. Girma, E.S. Kissel, A.N. Levy, S. MacCracken, P.R. Mastrandrea & L.L. White (eds.)]. Cambridge University Press, Cambridge, UK & New York, NY, USA, pp. 1199–1265.

Osborn, T.J. & P.D. Jones (2014). The CRUTEM4 land-surface air temperature data set: construction, previous versions and dissemination via Google Earth. *Earth Sys Sci Data* **6**, 61–68 (doi:10.5194/essd-6-61-2014**).**

Paltsev, S., C.A. Schlosser (lead authors); and Y.-H. Chen, X. Gao, A. Gurgel, H. Jacoby, J. Morris, R. Prinn, A. Sokolov & K. Strzepek (2021). Charting the Earth's Future Energy, Managed Resources, Climate, and Policy prospects – 2021 Global Change Outlook. MIT Joint Program on the Science and Policy of Global Change, https://globalchange.mit.edu/sites/default/files/newsletters/files/2021-JP-Outlook.pdf.

Pierce, D., T.P. Barnett, B. Santer & P.J. Gleckler (2009). Selecting global climate models for regional climate change studies. *PNAS* **106**(21): 8441–8446 (doi:10.1073/pnas.0900094106).

Reifen, C. & R. Toumi (2009). Climate projections: Past performance no guarantee of future skill? *Geophys. Res. Lett.* **36** (doi:10.1029/2009GL038082).

Reilly, J.M. *et al.* (2021). The Covid-19 effect on the Paris Agreement. *Humanities & Social Sciences Communications* **8**(16).

Santer, B.D., T.M.L. Wigley, M.E. Schlesinger & J.F.B. Mitchell (1990). Developing climate scenarios from equilibrium GCM results, *Tech. Rep.*, Max–Planck-Institut für Meteorologie, Hamburg, Germany.

Schlosser, C.A., A. Sokolov, K. Strzepek, T. Thomas, X. Gao & C. Arndt (2021). The changing nature of hydroclimatic risks across South Africa. *Clim. Change* **168**(28) (doi:10.1007/s10584-021-03235-5).

Schlosser, C.A. & K. Strzepek (2015). Regional climate change of the greater Zambezi River basin: a hybrid assessment. *Clim. Change* **130**:9–19.

Schlosser, C.A., X. Gao, K. Strzepek, A. Sokolov, C.E. Forest, S. Awadalla, W. Farmer (2012). Quantifying the Likelihood of Regional Climate Change: A Hybridized Approach. *J. Climate* **26**(10): 3394–3414 (doi:10.1175/JCLI-D-11-00730.1)

Sokolov, A., D. Kicklighter, A. Schlosser, C. Wang, E. Monier, B. Brown-Steiner, *et al.* (2018). Description and Evaluation of the MIT Earth System Model (MESM). *J. Adv. Model. Earth Sys.* **10**, 1759–1789 (doi:10.1002/2018MS001277).

Sousa, P.M., R. Blamey, C.J.C. Reason, A.M. Ramos & R.M. Trigo (2018). The 'Day Zero' Cape Town drought and the poleward migration of moisture corridors. *Environ. Res. Lett.* **13**(12): 124025 (doi:10.1088/1748-9326/aaebc7).

Taylor, K.E., R.J. Stouffe & G.A. Meehl (2012). An Overview of CMIP5 and the experiment design. *Bull. Amer. Meteor. Soc.* **93**, 485–498 (doi:10.1175/BAMS-D-11-00094.1).

Thomas, T., *et al.* (2020). Climate change risks to crop yields over southern Africa (forthcoming paper).

Wigley, T.M.L., S.C.B. Raper, S. Smith & M. Hulme (2000). *The MAGICC/SCENGEN Climate Scenario Generator: Version 2.4: Technical Manual*, CRU, UEA, Norwich, U.K.

# Joint Program Report Series - Recent Articles

For limited quantities, Joint Program Reports are available free of charge. Contact the Joint Program Office to order.
Complete list: http://globalchange.mit.edu/publications

368. **The Changing Nature of Human-Forced Hydroclimatic Risks across Africa.** *Schlosser et al., Aug 2023*

367. **Quantifying the recreation use value of New England natural lands.** *Lin et al., Jul 2023*

366. **An investigation into the effects of border carbon adjustments on the Canadian economy.** *Chen et al., Jun 2023*

365. **Building a composite indicator for biodiversity through supervised learning and linked indicator sets.** *Rouge and Schlosser, Mar 2023*

364. **Temperature Implications of the 2023 Shell Energy Security Scenarios: Sky 2050 and Archipelagos.** *Sokolov et al., Mar 2023*

363. **A Large Ensemble Global Dataset for Climate Impact Assessments.** *Gao et al., Feb 2023*

362. **SEBALIGEE v2: Global Evapotranspiration Estimation Replacing Hot/Cold Pixels with Machine Learning.** *Mhawej et al., Oct 2022*

361. **Assessing Compounding Risks Across Multiple Systems and Sectors: A Socio-Environmental Systems Risk-Triage Approach.** *Schlosser et al., Sep 2022*

360. **The MIT EPPA7: A Multisectoral Dynamic Model for Energy, Economic, and Climate Scenario Analysis.** *Chen et al., Jun 2022*

359. **A Tool for Air Pollution Scenarios (TAPS v1.0) to Facilitate Global, Long-term, and Flexible Study of Climate and Air Quality Policies.** *Atkinson et al., Jun 2022*

358. **Assessing the Changing Risk of Flood-producing Events in Cambridge.** *Gao & Schlosser, Mar 2022*

357. **The Changing Nature of Climate-Related Risks in Global Wind Power Resources.** *Schlosser et al., Feb 2022*

356. **Transition Scenarios for Analyzing Climate-Related Financial Risk.** *Chen et al., Jan 2022*

355. **Economic Analysis of the Hard-to-Abate Sectors in India.** *Paltsev et al., Sep 2021*

354. **Distributional Impacts of Low-Carbon Policies in USA and Spain: Does One Size Fit All?** *Garcia-Muros et al., Aug 2021*

353. **Predictability of U.S. Regional Extreme Precipitation Occurrence Based on Large-Scale Meteorological Patterns (LSMPs).** *Gao & Mathur, Jun 2021*

352. **Toward Resilient Energy Infrastructure: Understanding the Effects of Changes in the Climate Mean and Extreme Events in the Northeastern United States.** *Komurcu & Paltsev, Jun 2021*

351. **Meeting Potential New U.S. Climate Goals.** *Yuan et al., Apr 2021*

350. **Hydroclimatic Analysis of Climate Change Risks to Global Corporate Assets in Support of Deep-Dive Valuation.** *Strzepek et al., Apr 2021*

349. **A Consistent Framework for Uncertainty in Coupled Human-Earth System Models.** *Morris et al., Mar 2021*

348. **Changing the Global Energy System: Temperature Implications of the Different Storylines in the 2021 Shell Energy Transformation Scenarios.** *Paltsev et al., Feb 2021*

347. **Representing Socio-Economic Uncertainty in Human System Models.** *Morris et al., Feb 2021*

346. **Renewable energy transition in the Turkish power sector: A techno-economic analysis with a high-resolution power expansion model, TR-Power.** *Kat, Feb 2021*

345. **The economics of bioenergy with carbon capture and storage (BECCS) deployment in a 1.5°C or 2°C world.** *Fajardy et al., Nov 2020*

344. **Future energy: In search of a scenario reflecting current and future pressures and trends.** *Morris et al., Nov 2020*

343. **Challenges in Simulating Economic Effects of Climate Change on Global Agricultural Markets.** *Reilly et al., Aug 2020*

342. **The Changing Nature of Hydroclimatic Risks across South Africa.** *Schlosser et al., Aug 2020*

341. **Emulation of Community Land Model Version 5 (CLM5) to Quantify Sensitivity of Soil Moisture to Uncertain Parameters.** *Gao et al., Feb 2020*

340. **Can a growing world be fed when the climate is changing?** *Dietz and Lanz, Feb 2020*

339. **MIT Scenarios for Assessing Climate-Related Financial Risk.** *Landry et al., Dec 2019*

338. **Deep Decarbonization of the U.S. Electricity Sector: Is There a Role for Nuclear Power?** *Tapia-Ahumada et al., Sep 2019*

337. **Health Co-Benefits of Sub-National Renewable Energy Policy in the U.S.** *Dimanchev et al., Jun 2019*

336. **Did the shale gas boom reduce US $CO_2$ emissions?** *Chen et al., Apr 2019*

**MIT Joint Program on the Science and Policy of Global Change**

Massachusetts Institute of Technology
77 Massachusetts Ave., E19-411
Cambridge MA 02139-4307 (USA)

**T** (617) 253-7492 **F** (617) 253-9845
globalchange@mit.edu
http://globalchange.mit.edu/